

Development and verification of a novel disulfidptosis-related lncRNA prognostic model for predicting the immune environment and treatment of breast cancer

Qinghua Zhang¹, Guizhen Pan^{2*}, Tingting Wang³, Jiqing Hao^{1*}

¹Department of Oncology, The First Affiliated Hospital of Anhui Medical University, Anhui, China

²Department of Radiation Oncology, The First Affiliated Hospital of Anhui Medical University, Anhui, China

³Department of Intensive Care Unit, West District of The First Affiliated Hospital of University of Science and Technology of China, Division of Life Sciences and Medicine, University of Science and Technology of China, Anhui, China

Submitted: 26 September 2024; **Accepted:** 17 March 2025

Online publication: 25 April 2025

Arch Med Sci

DOI: <https://doi.org/10.5114/aoms/203010>

Copyright © 2025 Termedia & Banach

Abstract

Introduction: Breast cancer is the leading cause of cancer-related death in women. Disulfidptosis is a recently identified type of cell death that may offer new opportunities for cancer treatment. However, it is uncertain whether disulfidptosis-related lncRNAs (DRlncRNAs) are associated with BRCA.

Material and methods: We first evaluated the expression of disulfidptosis-related genes (DRGs) by RT-PCR. We then identified DRlncRNAs using Pearson's correlation, followed by univariate regression to select prognosis-related genes. LASSO regression and multivariate Cox regression were used to construct a prognostic model, and ROC curves were used to evaluate the model's predictive performance. We compared infiltration of various immune cells and expression of immune checkpoint genes between risk groups. Maftools was employed to analyze the tumor mutation burden (TMB) of patients. Finally, the pRRophetic package was used to analyze the sensitivity of patients to anticancer drugs.

Results: We found that OXSM, RPN1, SLC3A2, and SLC7A11 showed increased expression levels in tumor tissues compared to normal tissues. We then constructed and validated a prognostic model (AC007996.1, AC004816.2, MIR200CHG, AL354920.1). Patients in the high-risk group had significantly reduced percentages of naive B cells and CD8+ T cells, and higher expression levels of immune checkpoint-related genes compared to patients in the low-risk group, suggesting immune escape ability of the high-risk group. Patients in the high-risk group had a higher TMB. Finally, patients in the high-risk group had higher IC₅₀ values for many targeted agents, suggesting poor drug sensitivity.

Conclusions: We identified DRG expression in breast cancer, and constructed a prognostic model predicting the prognosis, the immune microenvironment, TMB, and drug sensitivity.

Key words: disulfidptosis, breast cancer, lncRNA, immune checkpoint genes, prognostic model.

*Corresponding authors:

Guizhen Pan
Department of Radiation
Oncology,
The First Affiliated
Hospital of Anhui
Medical University
Anhui, China
E-mail: penguin2521@163.
com

Jiqing Hao
Department of Oncology
The First Affiliated
Hospital of Anhui
Medical University
81 Meishan Road
Hefei, 230022, China
Phone: +86 13965029739
E-mail: haojiqing@ahmu.
edu.cn

Introduction

BRCA presents a significant threat to women's health, as evidenced by the latest survey, which reported approximately 287,850 new BRCA

diagnoses in 2022 [1]. Over the past few decades, the incidence of female BRCA has experienced a steady increase, growing at a rate of approximately 0.5% annually since the mid-2000s [2]. However, BRCA displays considerable heterogeneity in response to therapeutic interventions, making accurate prognosis a challenging task. In clinical practice, prognostic indicators for BRCA patients have traditionally relied on factors such as tumor stage, histological grade, and molecular subtype [3, 4]. Unfortunately, the predictive accuracy of these clinical characteristics remains sub-optimal. Consequently, there is a pressing need to explore the evolving molecular landscape of BRCA, identify updated prognostic biomarkers, and develop more advanced therapeutic strategies.

Long non-coding RNAs (lncRNAs) have emerged as pivotal regulators of protein-coding genes, with increasing evidence suggesting their involvement in cancer development and progression [5]. More and more studies have constructed lncRNA models to predict patients with cancers [6, 7]. The relationship between BRCA and lncRNAs has garnered substantial attention in recent years. Notably, several lncRNAs, including HOTAIR [8], H19 [9], and DSCAM-AS1 [10], have been identified as crucial players in predicting treatment outcomes, metastasis, and prognosis in BRCA. Furthermore, lncRNAs have been implicated in modulating the immune response and influencing the effectiveness of immunotherapy by regulating the PD-1/PD-L1 pathway [11]. Consequently, lncRNAs hold promise as potential prognostic factors and therapeutic targets for BRCA.

Programmed cell death plays a pivotal role in tumorigenesis and is particularly relevant in the context of metabolic cancer therapy, such as cuproptosis, a novel cell death mechanism [12], which has shown promise in various cancer types. A recent study [13] revealed a novel regulated cell death process termed “disulfidptosis” in kidney cancer cells. This process is characterized by the upregulation of solute carrier family 7 member 11 (SLC7A11), leading to the depletion of cytoplasmic nicotinamide adenine dinucleotide phosphate (NADPH) under conditions of glucose deprivation. Consequently, disulfide molecules accumulate, triggering the formation of disulfide bonds between actin cytoskeleton proteins and causing disintegration of the actin filament (F-actin) network. This ultimately results in disulfide stress and disulfidptosis. Genome-wide CRISPR-Cas9 screening identified ten genes (GYS1, NDHFS1, OXSM, LRP-PRC, NDUFA11, NUBPL, NCKAP1, RPN1, SLC3A2, and SLC7A11) associated with disulfidptosis [13]. This groundbreaking study suggests that disulfidptosis may offer a novel target for cancer therapy. However, to date, limited research has explored the connection between disulfidptosis and BRCA.

In our research, we developed a prognostic model for BRCA based on four differentially expressed disulfide-related lncRNAs (DRlncRNAs). Additionally, we explored the immune landscape of the tumor microenvironment (TME), assessed tumor mutation burden (TMB), and predicted medication therapy responses using various risk scores.

Material and methods

Data acquisition and processing

We collected a total of 940 tumor samples and 95 normal samples from patients with BRCA from the TCGA website (<https://portal.gdc.cancer.gov/>). We also obtained corresponding clinical details and somatic mutation data. Using the ‘create-DataPartition’ function, we randomly divided the 922 BRCA patients with survival information into a training group ($N = 554$) and a testing group ($N = 368$) at a 6 : 4 ratio for subsequent model development and validation. A χ^2 test was conducted to ensure a balanced distribution of clinicopathological factors between the training and testing cohorts. No significant differences in clinical characteristics were observed between the groups, as summarized in Table I. Furthermore, research by Liu *et al.* [13] identified a set of ten genes related to disulfidptosis (DRGs), which we considered in our study.

Identification of disulfidptosis-related genes and creation of subgroups

We utilized the “limma” package to analyze the levels of ten DRGs in tumor and normal tissues with a screening threshold of $p < 0.05$. To identify molecular subtypes of BRCA associated with disulfidptosis, consensus clustering was performed using the k-means method via the ‘Consensus-ClusterPlus’ package in R software, based on the expression of DRGs. Subsequently, expression profiles of DRGs between the disulfidptosis-related subgroups were compared using differential expression analysis of the “limma” package. The disparities in the prognosis among groups in the Kaplan-Meier (K-M) survival curves were assessed using the log rank method. With $p < 0.05$ and $|\log_2(\text{fold change})| > 1$ as the screening threshold, a differential analysis of subgroups was conducted by the “limma” package to identify differentially expressed genes (DEGs). The “clusterProfiler” package of R software was then used to conduct Gene Ontology (GO) and Kyoto Encyclopedia of Genes and Genomes (KEGG) studies on DEGs ($p < 0.05$). Based on the TCGA-BRCA cohort, 22 immune cell infiltrations were calculated in each BRCA sample using the CIBERSORT method. Finally, the immune score, stromal score, and estimate score were determined for each in the TCGA-BRCA

Table I. Clinical information in the training, testing, and entire groups

Characteristics	Type	Entire group (N = 922)	Testing group (N = 368)	Training group (N = 554)	P-value
Age	≤ 65	648 (70.28%)	264 (71.74%)	384 (69.31%)	0.474
	> 65	274 (29.72%)	104 (28.26%)	170 (30.69%)	
Stage	Stage I	153 (16.59%)	57 (15.49%)	96 (17.33%)	0.697
	Stage II	523 (56.72%)	210 (57.07%)	313 (56.5%)	
	Stage III	210 (22.78%)	87 (23.64%)	123 (22.2%)	
	Stage IV	17 (1.84%)	5 (1.36%)	12 (2.17%)	
	Unknown	19 (2.06%)	9 (2.45%)	10 (1.81%)	
T	T1	240 (26.03%)	87 (23.64%)	153 (27.62%)	0.314
	T2	533 (57.81%)	225 (61.14%)	308 (55.6%)	
	T3	113 (12.26%)	41 (11.14%)	72 (13%)	
	T4	33 (3.58%)	15 (4.08%)	18 (3.25%)	
	Unknown	3 (0.33%)	0 (0%)	3 (0.54%)	
M	M0	767 (83.19%)	309 (83.97%)	458 (82.67%)	0.948
	M1	19 (2.06%)	7 (1.9%)	12 (2.17%)	
	Unknown	136 (14.75%)	52 (14.13%)	84 (15.16%)	
N	N0	427 (46.31%)	168 (45.65%)	259 (46.75%)	0.735
	N1	313 (33.95%)	126 (34.24%)	187 (33.75%)	
	N2	101 (10.95%)	38 (10.33%)	63 (11.37%)	
	N3	63 (6.83%)	29 (7.88%)	34 (6.14%)	
	Unknown	18 (1.95%)	7 (1.9%)	11 (1.99%)	

cohort using the ESTIMATE method in R software, and the differences in these scores between subgroups were further assessed by the Wilcoxon test.

Construction of a disulfidptosis-related lncRNA model

Using strawberry perl (<https://strawberryp Perl.com/>) software, lncRNAs were screened from TCGA-BRCA RNA expression profiles. Disulfidptosis-related lncRNAs (DRlncRNAs) were identified using Pearson correlation analysis, with thresholds set at $|R| > 0.3$ and $p < 0.001$ between the ten DRGs and lncRNAs. These thresholds are widely utilized in similar studies exploring gene-gene or gene-lncRNA correlations in cancer research, ensuring both biological relevance and statistical rigor [14, 15]. Univariate Cox regression analysis was used in the training group to identify DRlncRNAs related to prognosis.

Later on, the least absolute shrinkage and selection operator (LASSO) regression with cross-validation was performed to identify the most predictive lncRNAs from a larger dataset, thereby enhancing the accuracy and robustness of the model. Finally, the lncRNAs identified by LASSO were subjected to stepwise multivariate Cox proportional hazards regression analysis to identify the optimal candidates and construct a disulfidptosis-related lncRNA prognosis prediction model.

The risk score formula of the model based on multivariate Cox regression was as follows: $\text{Risk score} = \text{expression}_{\text{gene1}} \times \beta_{\text{gene1}} + \text{expression}_{\text{gene2}} \times \beta_{\text{gene2}} + \text{expression}_{\text{genex}} \times \beta_{\text{genex}}$

The risk score for every BRCA patient was calculated using the risk score formula and classified BRCA patients into high-risk and low-risk categories using the median value. Risk score curves, survival status point plots, and risk lncRNA heat maps were created in the training group, testing group, and entire group to examine the link between the risk score and prognosis. K-M curves of overall survival between high and low-risk groups were developed to further explore the prognostic value of the model. The independent prognostic value of the risk score was evaluated through univariate and multivariate Cox regression analyses using the “survival” R package. The receiver operating characteristic (ROC) curve and the area under the curve (AUC) were employed to assess the prediction accuracy of the risk model via the R “timeROC” package. In addition, the C-index for clinicopathological factors and the risk score was calculated for the entire group.

Nomogram and principal component analysis (PCA)

A nomogram is a graphical tool that is designed to approximate complicated calculations quickly

and without a computer or calculator. It has been widely used for decades to predict clinical outcomes based on statistical models in most types of cancer. A nomogram was established using the R package ‘rms’ based on the risk score and clinical factors. Then, the predictive effect of the nomogram was validated by the calibration curve. In addition, the decision curve analysis (DCA) curve was developed to evaluate the clinical applicability of the risk model and nomogram via the DCA package in R software. PCA is a widely used tool for dimensionality reduction and feature extraction in the computer vision field. PCA based on DRGs, all genes, risk lncRNAs, and DRlncRNAs was carried out on all BRCA patients using the “scatterplot3d” package to determine the capacity of these gene sets to distinguish patients with high and low risk scores.

Gene set enrichment analysis

To explore potential biological mechanisms that might account for the prognostic difference between the two risk groups, the file “c2.cp. Kegg.symbols.gmt” was obtained from the MSigDB database (<https://www.gsea-msigdb.org/gsea/msigdb>). Gene set enrichment analysis (GSEA) analysis was carried out by applying the “clusterProfiler” package of R software ($p < 0.05$) to obtain enriched pathways in high- and low-risk groups.

Immune microenvironment analysis

According to the immune score, stromal score, and estimate score of each sample in the TCGA-BRCA cohort, differences in these scores between the two risk groups were analyzed using the Wilcoxon test. Using the immune cell infiltration in the TCGA-BRCA cohort calculated by the CIBERSORT method, between high-risk and low-risk groups, we examined the variations in immune cell infiltration. Additionally, a differential analysis of common immune checkpoint genes was also performed.

Somatic mutation calculation and drug sensitivity analysis

TMB was calculated for BRCA patients by processing the BRCA mutation data using Strawberry

software. The top 15 genes mutated in BRCA were analyzed between different risk groups using the “maftools” package and visualized by a waterfall diagram. Using the “survival” and “survminer” packages, further analysis revealed the relationship between TMB and survival. Statistical significance was defined as $p < 0.05$. The “oncoPredict” package was used to screen for sensitive drugs associated with risk scores at $p < 0.001$.

qRT-PCR identification of DRG expression in tissue samples

We collected a total of 18 samples from Anhui Provincial Hospital, comprising 9 BRCA pathological tissues and 9 para-tumor tissues. To identify differentially expressed DRGs at the pathological tissue level, we employed quantitative real-time PCR (qRT-PCR) technology. The primer sequences necessary for gene identification are shown in Table II. For RNA extraction, we used TRIzol reagent from Invitrogen, USA. Subsequently, qRT-PCR was conducted on the CFX96 Real-Time System C1000 Cycler from Bio-Rad Laboratories in Singapore. The qRT-PCR process involved the use of a reverse transcription kit from Takara, Japan, and a SYBR-Green PCR kit, also from Takara, Japan. Data analysis was performed utilizing the $2^{-\Delta\Delta Ct}$ method, and differences between the para-cancerous and BRCA samples were assessed through Student’s *t*-test. The studies involving human participants were reviewed and approved by Anhui Provincial Hospital (2023-ZNW-04).

Statistical analysis

All data were analyzed using the R software (R version: 3.6.1), strawberry perl software, and GraphPad Prism (version 10.0). The Wilcoxon test was used for nonparametric data and Student’s *t* test was used for parametric data in two individual groups. The chi-square test was used to compare categorical variables. Pearson’s correlation test was used to measure the linear association between two variables. Survival comparison was conducted using the log-rank test and visualized with KM curves. “limma”, “survival”, “timeROC”, “Rms”, “DCA”, and “scatterplot3d” were used for

Table II. Primer information of DRGs

Gene name	Forward primer	Reverse primer
NDUFA11	AGCTACAGCACCACCAGTATTG	TTGTCCAACCTTAGCTCCTTC
LRPPRC	CCTTGACACCGGCAAGTATG	CCTCTTAAAGCTGCGCCATT
NUBPL	TGCTGATGGTGCAAGGAAAAC	TTGGCTGGCCTGTATCTGAA
SLC7A11	TCAAATGCAGTGGCAGTGAC	AAACACACCACCGTTCATGG
OXSM	CACACCATTGGGAGATGCTG	CAGCAGATGTCTGTTGCTC
RPN1	AGCTCCCAGTTGCTCTTGAT	CTGACTGGGTGATCTGGGTT
SLC3A2	GGAGGTGGAGCTGAATGAGT	TCTCCGCCACCTTGATCTT

differential expression analysis, uni- and multi-Cox regression analyses, ROC curve construction, nomogram development, DCA curve establishment, and PCA, respectively. The CIBERSORT algorithm and ESTIMATE algorithm were employed in immune cell infiltration evaluation and TME score measurement, respectively. TMB was performed by the “maftools” package, and the “oncoPredict” package was used in drug sensitivity. Enrichment analysis was carried out via the “ClusterProfiler” package. A *p*-value of less than 0.05 was considered to be statistically significant.

Results

Classification of BRCA associated with disulfidptosis-related genes

Supplementary Figure S1 provides a flow chart illustrating the design of the research. Among the ten DRGs examined, seven displayed significant differences in expression between tumor tissues and para-tumor tissues within the TCGA-BRCA cohort (*p* < 0.01). Notably, LRPPRC, OXSM, RPN1, SLC3A2, NDUFA11, and SLC7A11 exhibited elevated expression levels in tumor tissues, whereas NUBPL demonstrated decreased expression in tumor tissues (Figure 1 A). Our qRT-PCR analysis

confirmed increased expression levels of OXSM, RPN1, SLC3A2, NDUFA11, and SLC7A11 in tumor tissues compared to normal tissues. In contrast, the expression levels of LRPPRC and NUBPL in tumor tissues showed no significant difference compared to their corresponding normal tissues (Figure 1 B). These initial findings led us to formulate the hypothesis that DRGs play a pivotal role in the context of BRCA. To investigate this hypothesis, we conducted a clustering analysis based on the expression profiles of the ten DRGs. We observed that when the consensus matrix reached *k* = 2, BRCA patients could be effectively grouped into two distinct clusters: cluster 1 and cluster 2. This clustering was accompanied by minimization of the slope of the cumulative distribution function (CDF) curve (Figure 1 C). Consequently, we proceeded to classify BRCA patients into two subgroups based on this clustering. Further analysis revealed that these subgroups exhibited distinct expression patterns for the DRGs. Cluster 1, characterized by high expression levels of many DRGs, was designated as the “high DRG group”. Conversely, cluster 2, with predominantly low expression of most DRGs, was labeled as the “low DRG group” (Figure 1 D). To explore the clinical relevance of these subgroups, we examined K-M

A

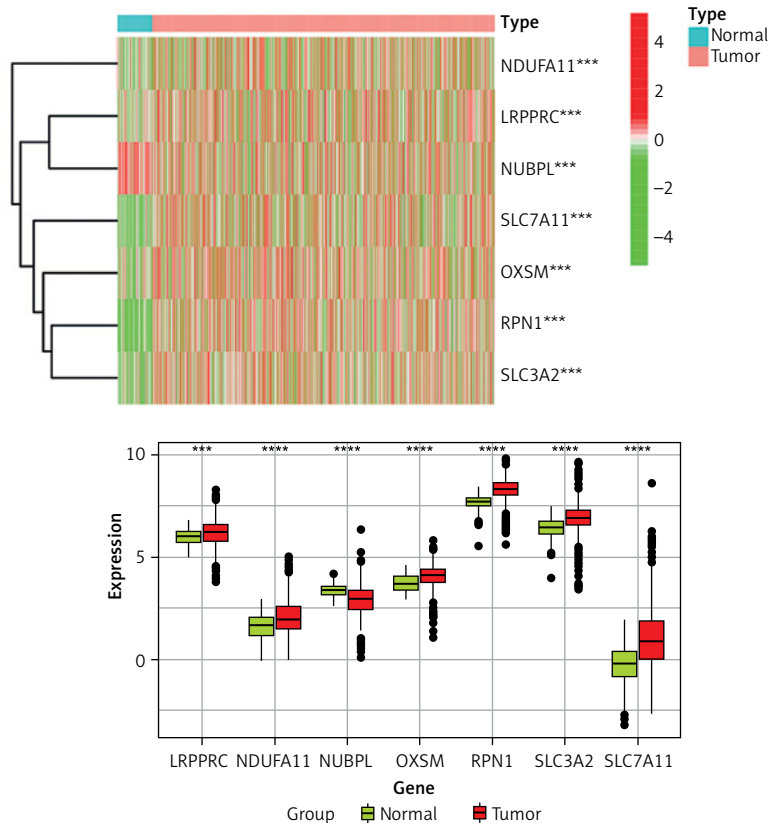


Figure 1. Differential analysis of DRGs and creation of DRG subgroups. **A** – Seven DRGs were significantly differentially expressed in tumor and normal tissues. **p* < 0.05; ***p* < 0.01, ****p* < 0.001

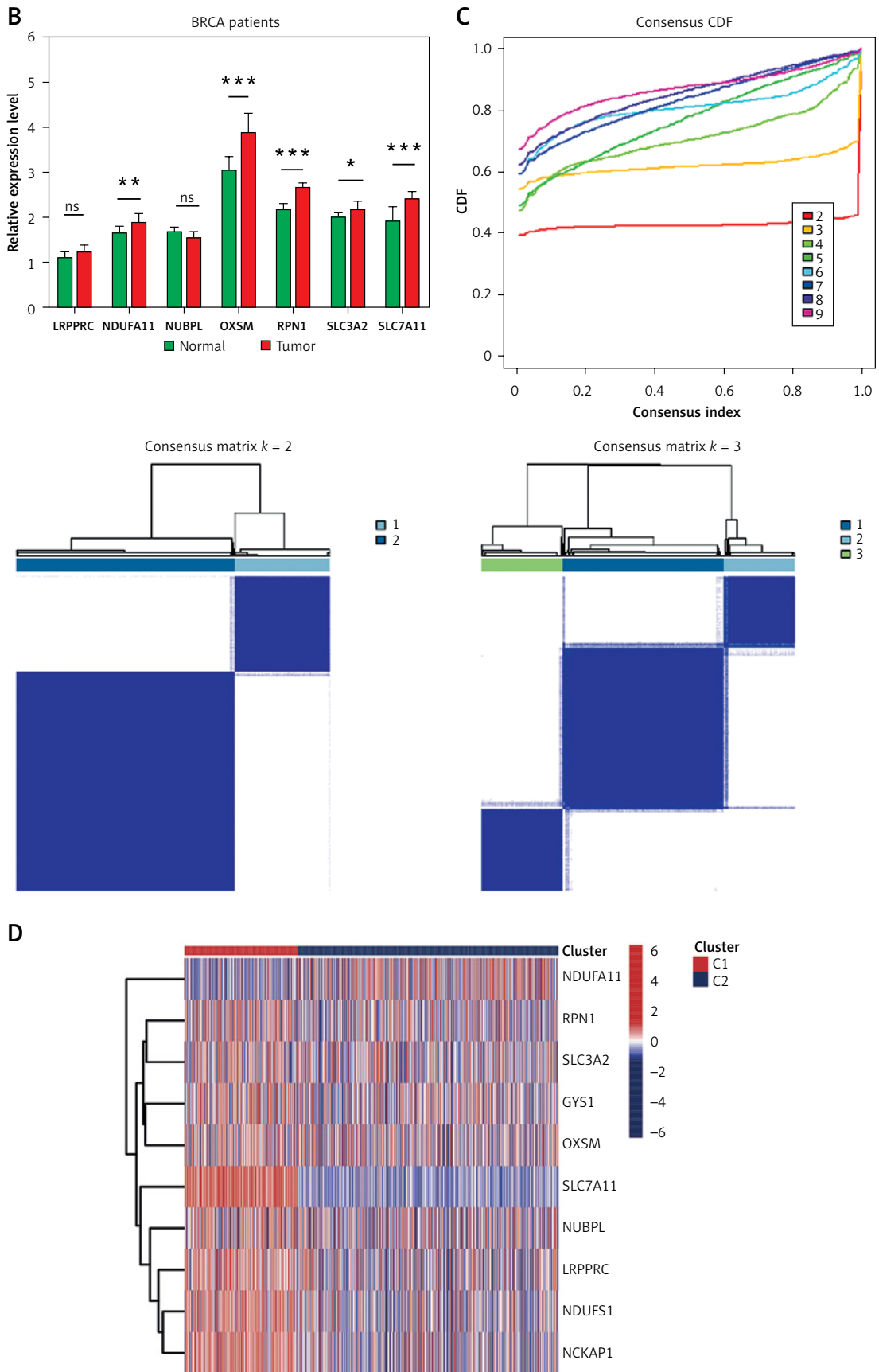


Figure 1. Cont. **B** – Expression levels of seven DRGs in tumor and para-tumor tissues identified by qRT-PCR, with Student’s t-test. **C** – The unsupervised clustering process, when $k = 2, 3$, and the CDF curve. When $k = 2$, the CDF curve was most moderate. **D** – Differences in expression levels of 10 DRGs in cluster 1 and cluster 2. * $p < 0.05$; ** $p < 0.01$, *** $p < 0.001$

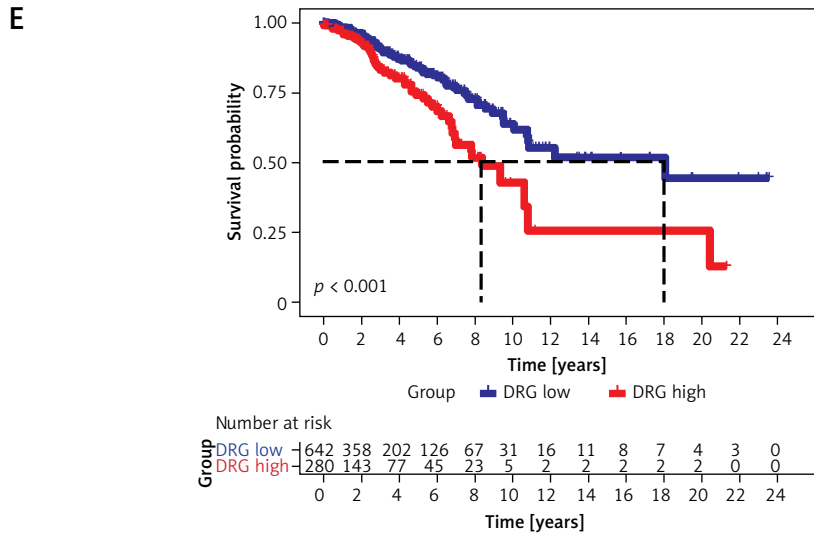


Figure 1. Cont. E – K-M survival curves in 2 subgroups. * $p < 0.05$; ** $p < 0.01$, *** $p < 0.001$

survival curves. These analyses indicated that patients in the low DRG group exhibited significantly better survival outcomes compared to those in the high DRG group ($p < 0.001$, Figure 1 E). These findings underscore the potential importance of DRGs in predicting patient prognosis in BRCA.

Functional enrichment and immune analysis of BRCA subgroups

Differential analysis was conducted on the two subgroups, resulting in the identification of 472

DEGs. Among these DEGs, 275 were up-regulated, and 197 were down-regulated. Subsequently, we performed GO enrichment for these DEGs across three functional classifications: Molecular Function (MF), Biological Process (BP), and Cellular Component (CC) (Figure 2 A). In the Molecular Function subontology, several GO terms related to critical biological functions were significantly enriched. These included antigen binding, endopeptidase activity, immunoglobulin receptor binding, gated channel activity, and serine hydrolase activ-

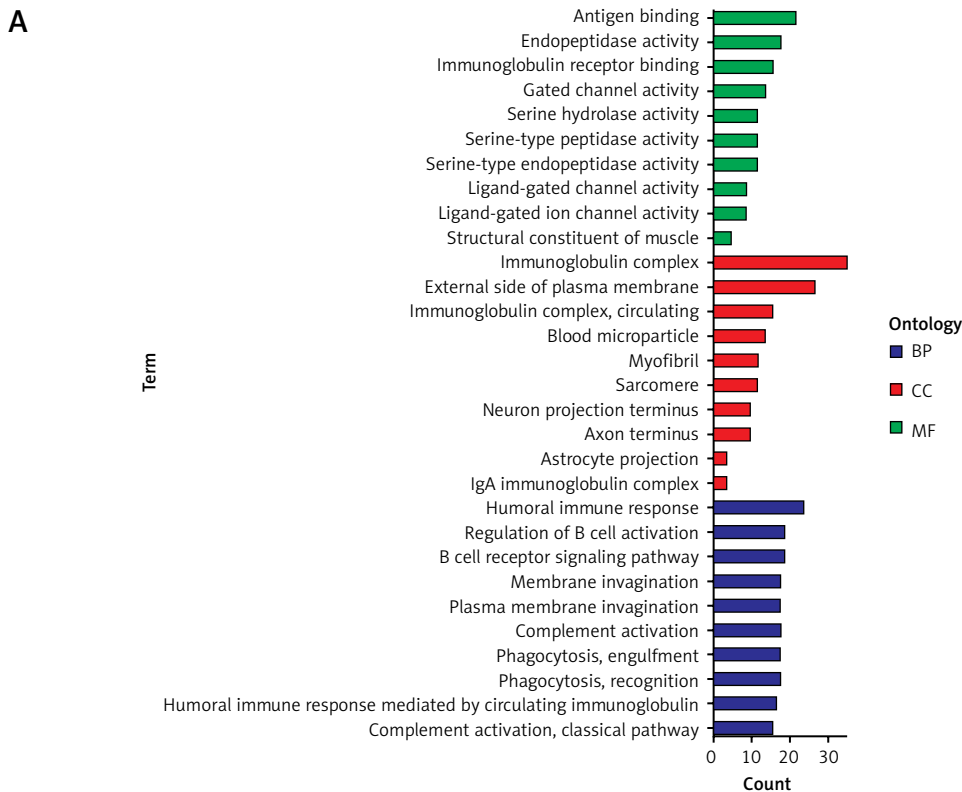
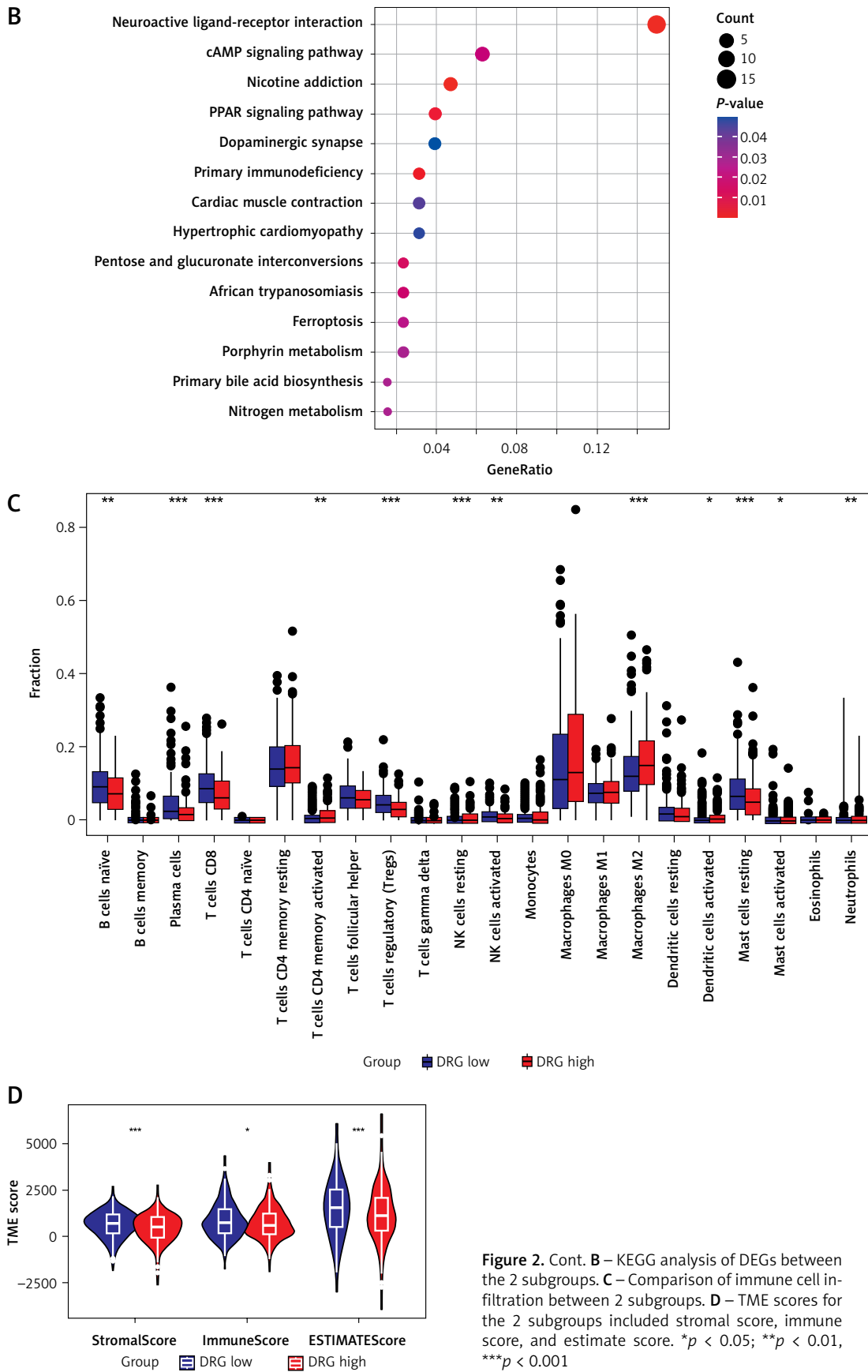


Figure 2. Enrichment analysis and immunoassay of DRG subgroups. **A** – GO analysis of DEGs between 2 subgroups. * $p < 0.05$; ** $p < 0.01$, *** $p < 0.001$



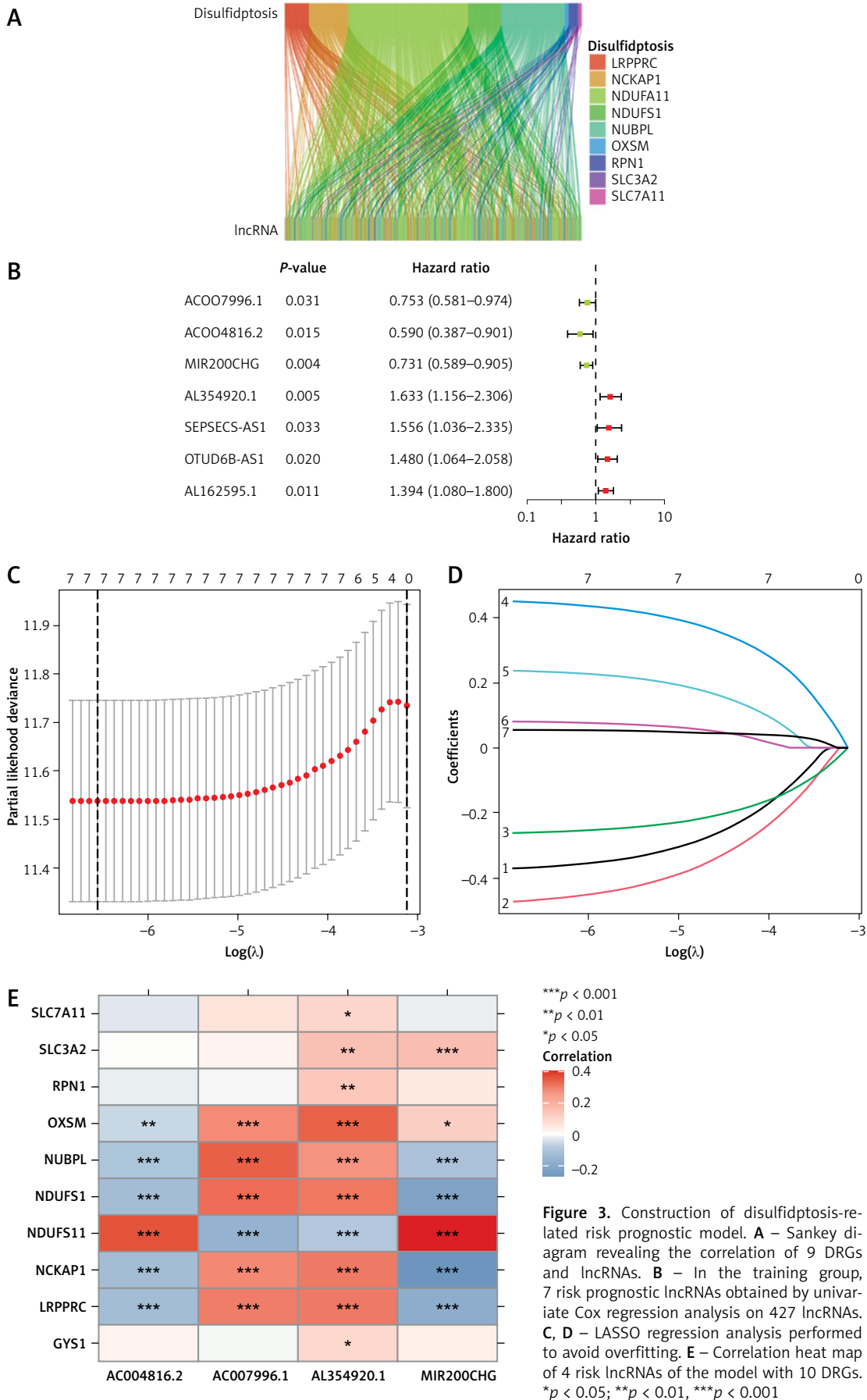
ity. Within the Biological Process category, we observed significant enrichment of GO terms associated with important processes such as humoral immune response, regulation of B cell activation, B cell receptor signaling pathway, membrane invagination, and plasma membrane invagination. In the Cellular Component classification, the enriched terms pointed to the involvement of DEGs in specific cellular locations and structures, such as the immunoglobulin complex, external side of the plasma membrane, circulating immunoglobulin complex, blood microparticle, and myofibril. Moreover, the KEGG pathway analysis indicated that these DEGs were notably enriched in several pathways, including neuroactive ligand-receptor interaction, the cAMP signaling pathway, nicotine addiction, the PPAR signaling pathway, the dopaminergic synapse, and primary immunodeficiency, among others (Figure 2 B). Notably, many of these pathways were related to immune functions and signaling. Subsequent immune cell infiltration analysis revealed intriguing insights. In the DRG low group, we observed higher infiltration levels of immune cells known for their tumor-suppressing and killing functions, including naïve B Cells, plasma cells, CD8⁺ T cells, Tregs, and activated NK cells. Conversely, the DRG high group exhibited elevated infiltration of M2 macrophages, a type of differentiated tumor-related macrophage, as well as resting NK cells (Figure 2 C). Furthermore, the analysis of TME scores demonstrated that the DRG low group exhibited higher immune scores and stromal scores, indicating a more pronounced immune response and stromal cell presence (Figure 2 D).

Construction and validation of prognostic model related to disulfidptosis in BRCA

In the Pearson correlation analysis, we found one DRG that correlated poorly with all lncRNAs, so we identified 427 lncRNAs that were correlated with 9 DRGs ($p < 0.001$ and $|R| > 0.3$). The Sankey diagram shows the correlation between DRGs and DRlncRNAs (Figure 3 A). In the training group, univariate Cox regression analysis identified 7 prognosis-related lncRNAs (Figure 3 B). Then, using LASSO regression and multivariate Cox regression analysis, we constructed a risk model composed of 4 lncRNAs (AC007996.1, AC004816.2, MIR200CHG, AL354920.1) (Figures 3 C, D). Based on the coefficients assigned to the 4 lncRNAs by the multivariate Cox regression, the risk score can be determined as: Risk score = expression_{AC007996.1} × β_{AC007996.1} + expression_{AC004816.2} × β_{AC004816.2} + expression_{MIR200CHG} × β_{MIR200CHG} + expression_{AL354920.1} × β_{AL354920.1}.

The correlation heat map (Figure 3 E) illustrates strong correlations between the four lncRNAs in-

cluded in the model and the ten DRGs. In all three groups – training, testing, and the entire groups – the risk score curves and survival status dot plots consistently showed that as the risk score increased, the prognosis worsened (Figures 3 F–H). Combining the risk score coefficients and the expression heat map of the four risk-associated lncRNAs, we observed that AC007996.1, AC004816.2, and MIR200CHG were strongly expressed and acted as protective factors for BRCA in the low-risk group. Conversely, AL354920.1, highly expressed in the high-risk group, served as a risk factor (Figures 3 F–H). The K-M survival curves demonstrated statistical significance in the training group ($p < 0.001$), testing group ($p = 0.003$), and the entire group ($p < 0.001$), indicating a worse prognosis in the high-risk group (Figures 4 A–C). These findings underscore the prognostic value of the model. Univariate Cox regression analysis was conducted in the training group ($p < 0.001$, HR = 1.629 (1.295–2.048)), testing group ($p = 0.005$, HR = 1.683 (1.172–2.415)), and the entire group ($p < 0.001$, HR = 1.652 (1.364–2.002)), revealing that the risk score was a significant prognostic factor (Figures 4 D–F). Furthermore, the results of multivariate Cox regression analysis in the training group ($p < 0.001$, HR = 1.543 (1.203–1.979)), testing group ($p = 0.012$, HR = 1.680 (1.120–2.520)), and the entire group ($p < 0.001$, HR = 1.541 (1.254–1.892)) suggested that the risk score remained an independent predictor of overall survival even after adjusting for other influencing factors (Figures 4 G–I). Additionally, the area under the ROC curve was calculated for 1-year, 3-year, and 5-year survival, resulting in values of 0.696, 0.675, and 0.651 in the training group; 0.734, 0.643, and 0.628 in the testing group; and 0.714, 0.655, and 0.641 in the entire group, respectively. These values indicated that the model maintained a stable and reliable predictive accuracy (Figures 4 J–L). Notably, the ROC curves also demonstrated that the 10-year C-index outperformed other clinical factors, underscoring the robust ability of the risk score to predict outcomes, particularly long-term outcomes (Figure 5 A). Additionally, we compared the 10-year concordance index (C-index) and area under the curve (AUC) values of our model with those of several existing disulfidptosis-related models. As shown in Figure 5 B and Supplementary Table SI, our model achieved a higher C-index than those developed by Wang *et al.* [16] (0.70 vs. 0.63), Zheng *et al.* [17] (0.70 vs. 0.67), and Liu *et al.* [18] (0.70 vs. 0.64). Regarding the AUC values for 1, 3, and 5 years, our model is similar to those of Chen *et al.* [19] and Wang *et al.* [16], but the models by Zheng *et al.* [17], Liu *et al.* [18], and Wu *et al.* [20] showed higher AUC values for these time points. These results suggest that,



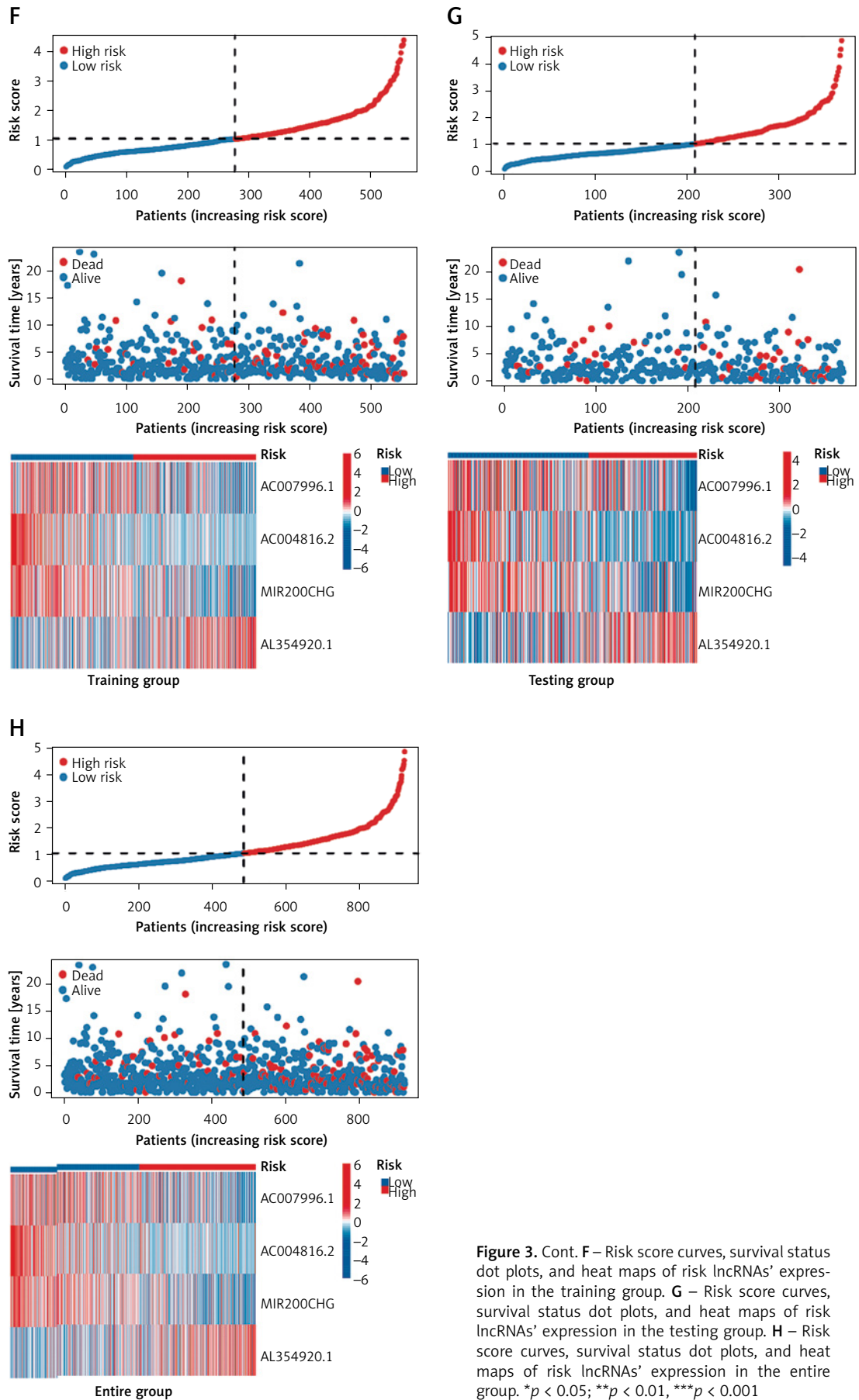


Figure 3. Cont. **F** – Risk score curves, survival status dot plots, and heat maps of risk lncRNAs' expression in the training group. **G** – Risk score curves, survival status dot plots, and heat maps of risk lncRNAs' expression in the testing group. **H** – Risk score curves, survival status dot plots, and heat maps of risk lncRNAs' expression in the entire group. * $p < 0.05$; ** $p < 0.01$; *** $p < 0.001$

while our model demonstrated superior predictive accuracy for 10-year overall survival (OS) in breast cancer patients, it showed slightly weaker performance in predicting OS during the first 5 years compared to some other models.

Nomogram and principal component analysis (PCA) in prognostic model

To enhance the impact of this model on clinical decision-making, we integrated the prognostic

risk-scoring model with current clinical parameters to develop a nomogram. The calibration curves, which demonstrated the agreement between predicted survival and actual clinical outcomes, confirmed the reliability of the nomogram's predictions (Figures 5 C, D). Additionally, the DCA curve showed that the nomogram has significant potential for clinical decision-making, outperforming the risk score and stage individually (Figure 5 E). To further validate the discriminative power of the

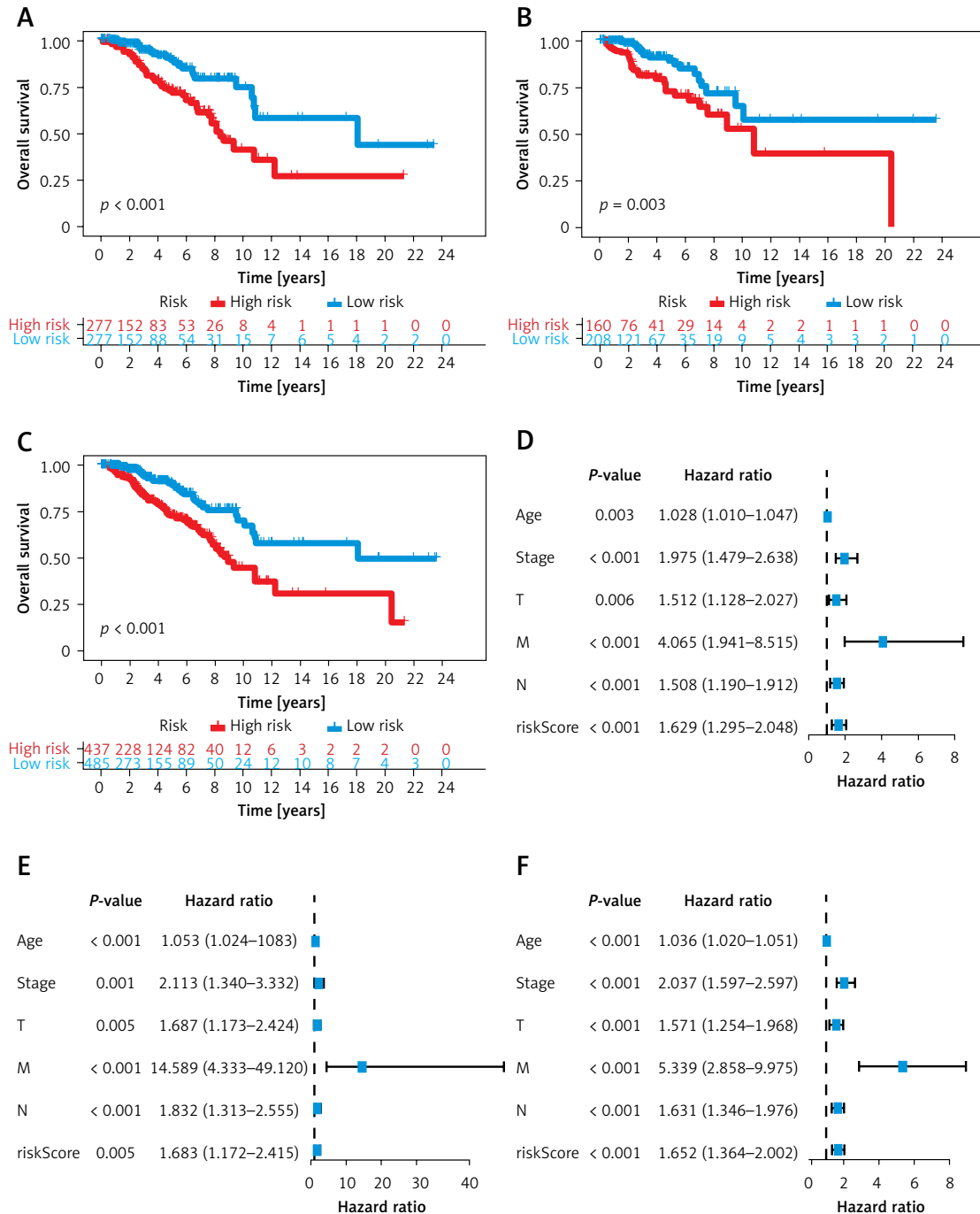


Figure 4. Validation and evaluation of risk prognostic model. **A–C** – K-M survival curve in the training group, testing group, and entire group. **D–F** – Univariate Cox regression in the training group, testing group, and entire group

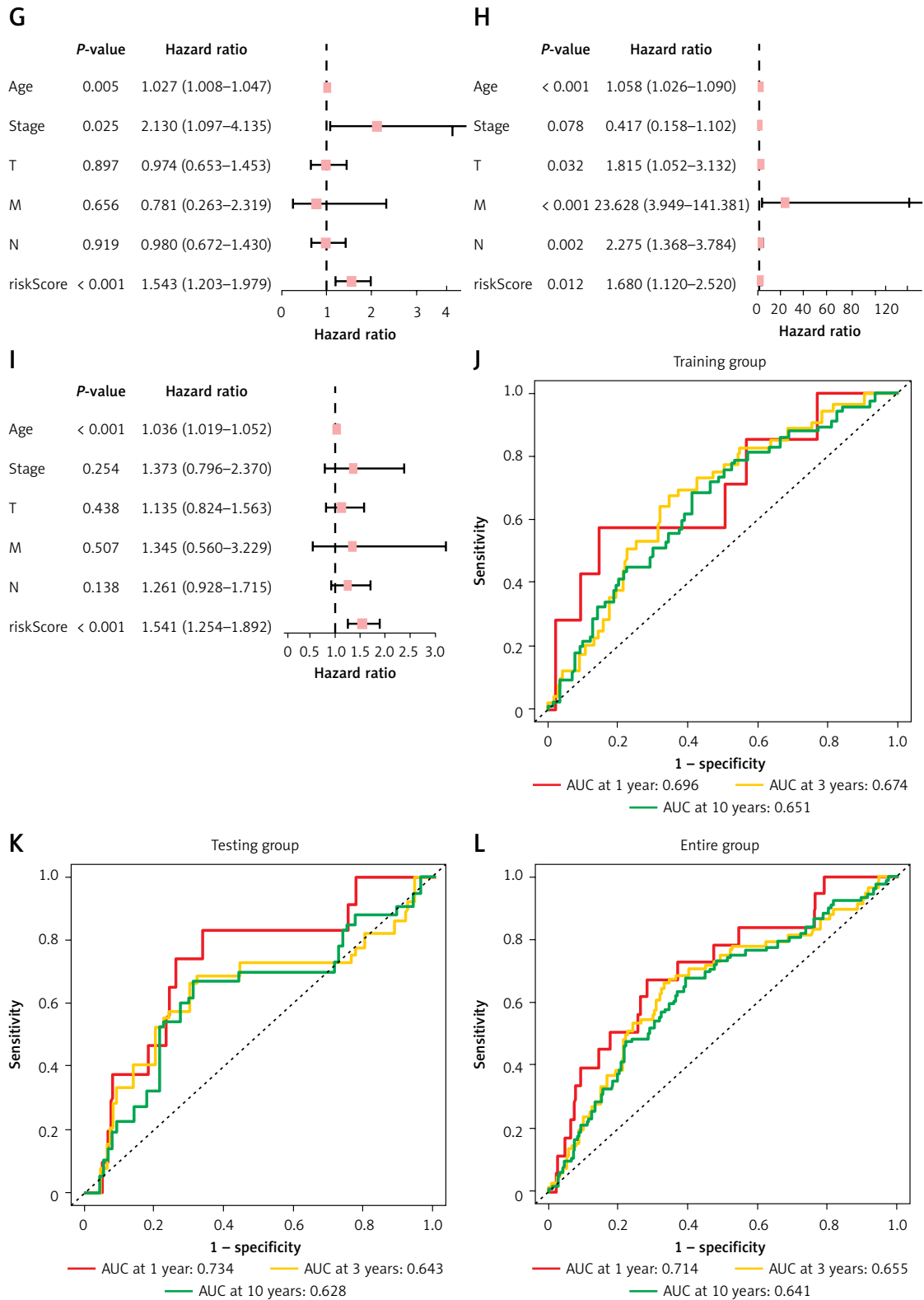


Figure 4. Cont. G–I – Multivariate Cox regression for independent prognostic analysis in the training group, testing group, and entire group. J–L – AUC values of ROC curves in 1, 3, 5 years in the training group, testing group, and entire group

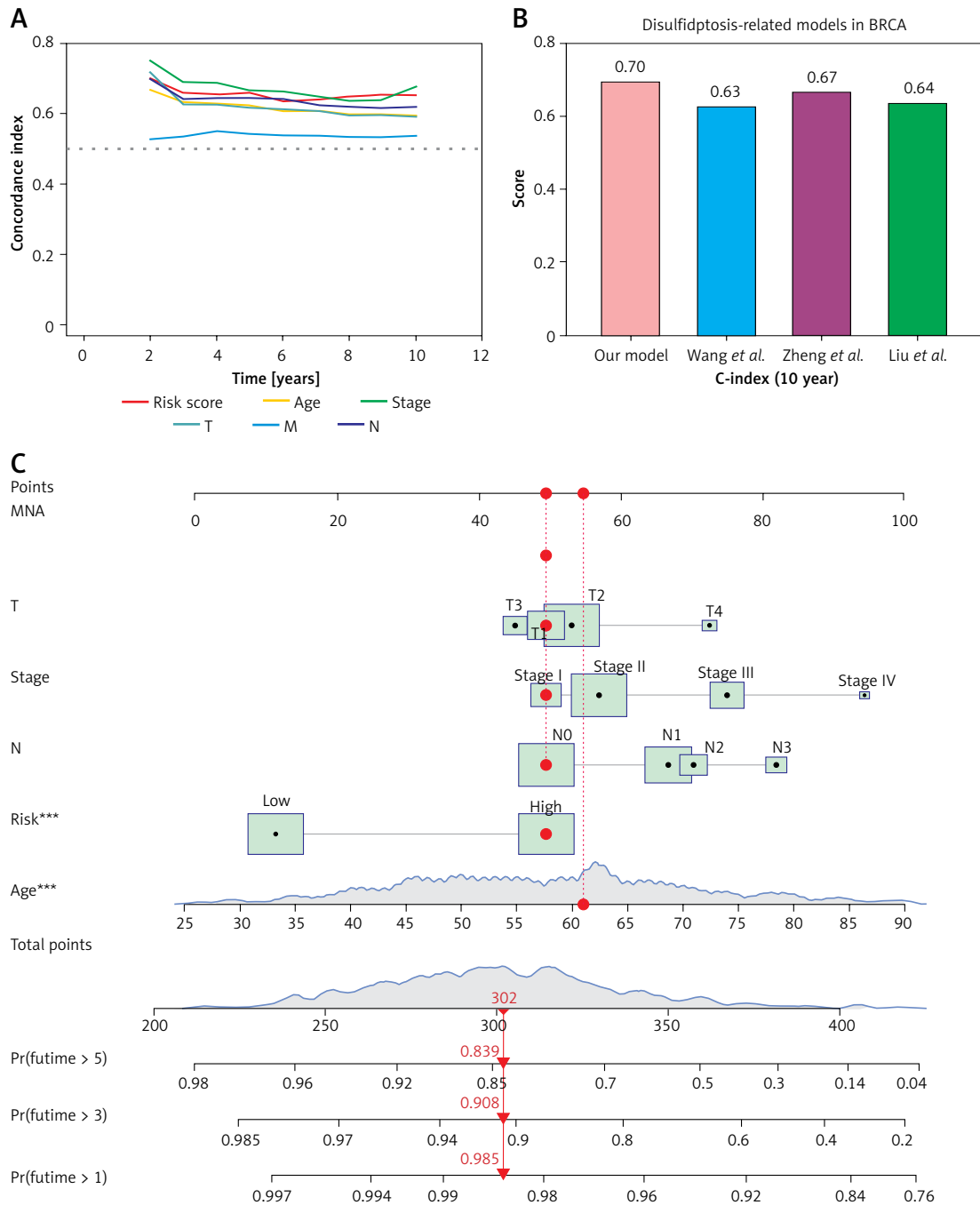


Figure 5. Nomogram and PCA. **A** – Comparison of the C-index of risk score and clinicopathological factors, including age, stage, T, M, and N. **B** – Comparison of C-index in disulfidptosis-related lncRNA prognostic models. **C** – Nomogram of the model obtained by combining risk scores and clinicopathological factors

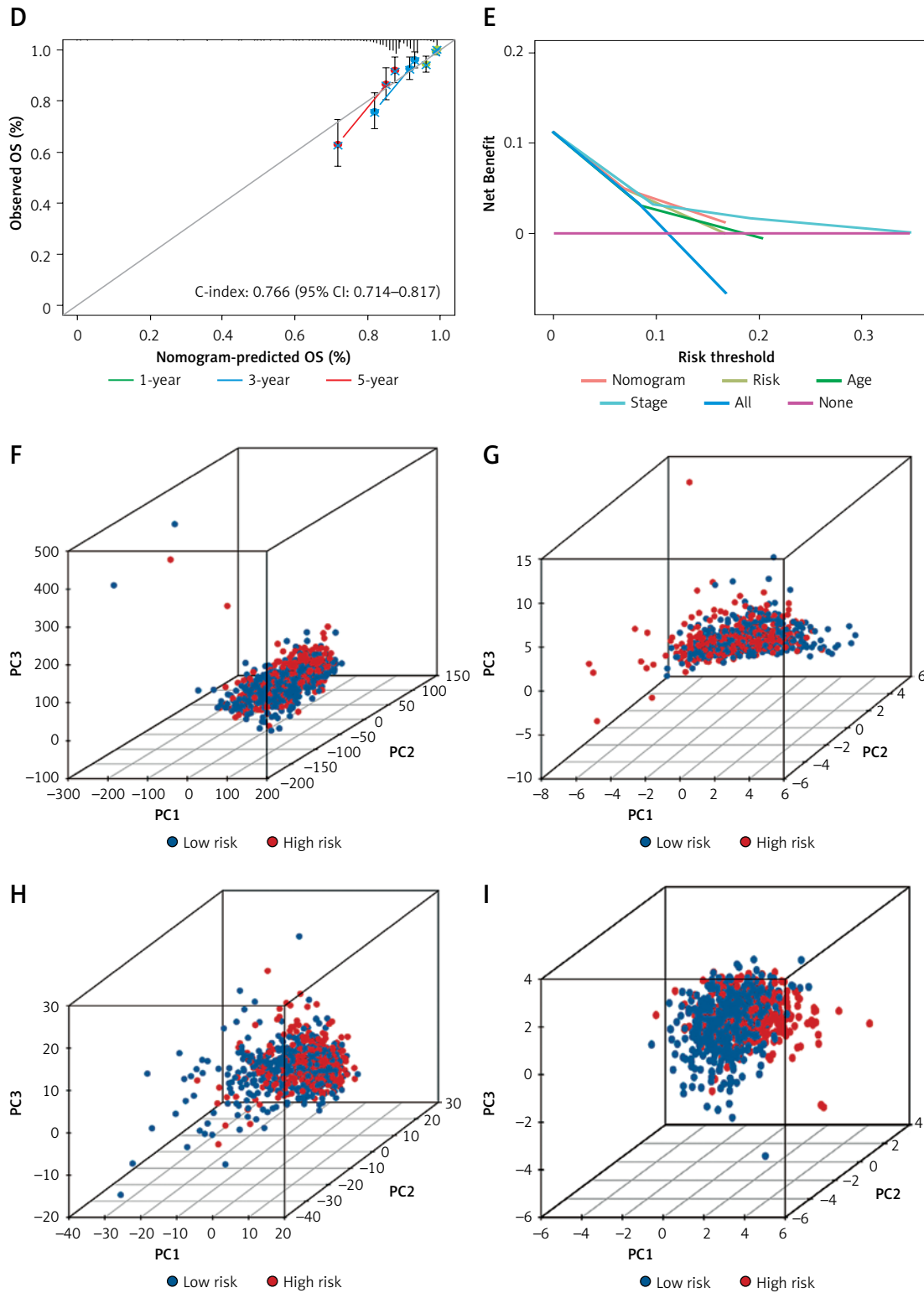


Figure 5. Cont. **D** – Calibration curve of nomogram in the model. **E** – DCA curve comparing the net benefit of the nomogram with the other variables included in the nomogram alone. * $p < 0.05$; ** $p < 0.01$, *** $p < 0.001$. **F–I** – PCA of TCGA-BRCA cohort based on all genes, DRGs, DRlncRNAs, and risk lncRNAs, respectively

model, we compared the distributions of entire gene sets, DRGs, DRlncRNAs, and the risk model between different risk groups using principal component analysis (PCA). As depicted in Figures 5 F-I, the four lncRNAs included in the model exhibited superior discriminatory ability in distinguishing the two risk groups compared to the entire gene sets, DRGs, or DRlncRNAs. These findings collectively provided robust support for the notion that this innovative prognostic model could accurately predict the prognosis of BRCA patients.

The correlation of clinical features and risk score

The statistical significance of the risk score extended beyond overall survival (OS) and encompassed progression-free survival (PFS) as well ($p < 0.001$), as illustrated in Figure 6 A. To further validate the prognostic relevance of the risk score, we analyzed various clinicopathological factors. Our findings consistently demonstrated that high-risk patients experienced poorer prognoses than their low-risk counterparts across a range of pathological factors, including age, T, N, M, and stage (Figure 6 B and Supplementary Figure S2). Sub-

sequently, we performed a correlation analysis to assess the relationship between the risk score and various clinicopathological factors. Notably, we observed a positive correlation between the risk score and T, indicating a connection between the risk score and tumor progression. Furthermore, patients classified as M1, denoting the presence of distant metastasis, exhibited higher risk scores, underscoring the predictive capacity of high-risk scores for tumor metastasis. Additionally, as patients progressed from stage I to stage IV, their risk scores increased (Figure 6 C). These comprehensive analyses provided further evidence of the prognostic significance of the risk score and its potential utility in predicting outcomes across various clinicopathological factors in BRCA patients.

Functional enrichment analysis in high- and low-risk group

To better understand how DRlncRNAs affected the occurrence and progression of BRCA, we performed GSEA analysis. The results revealed that gene sets of patients in the high-risk group were enriched in steroid biosynthesis, galactose metabolism, and ECM receptor interaction. There

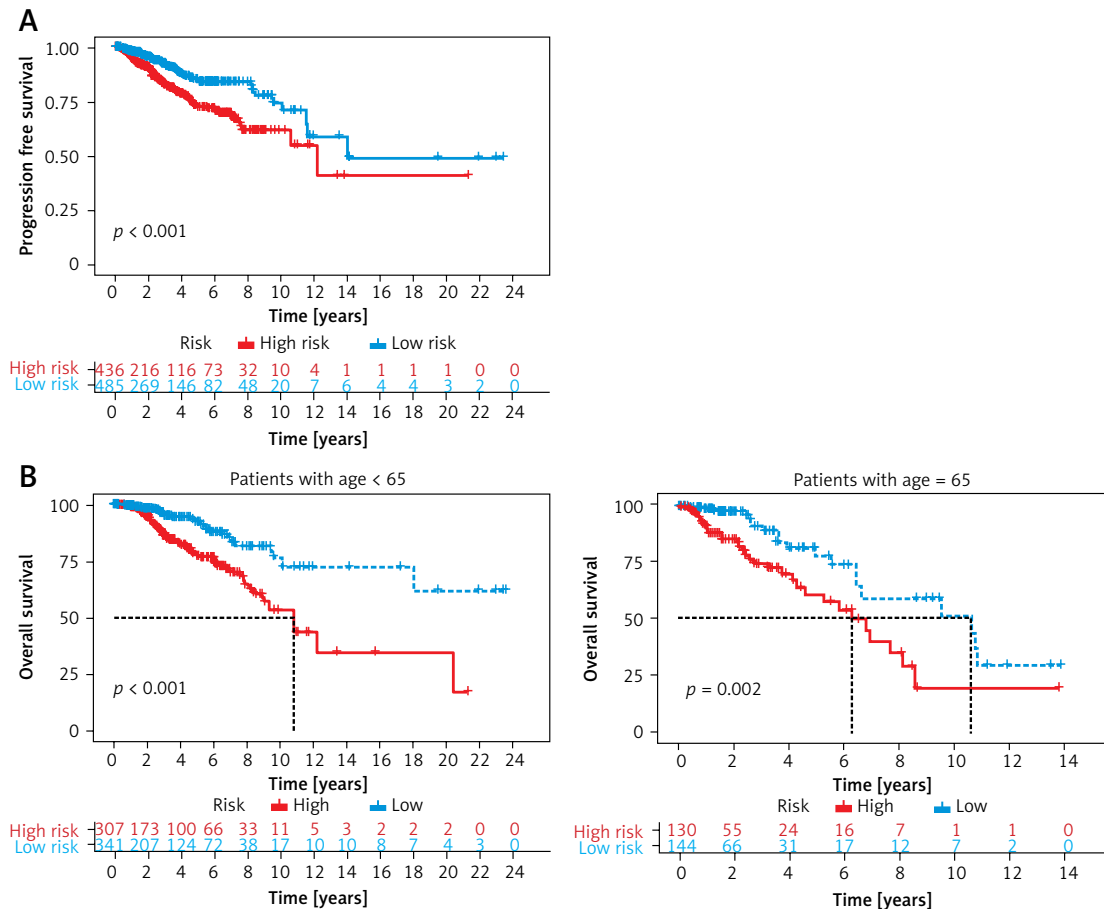


Figure 6. Risk-prognosis model and clinical correlation analysis. **A** – K-M curves of PFS in high- and low-risk groups. **B** – K-M curves for 2 risk groups in cohorts of different ages

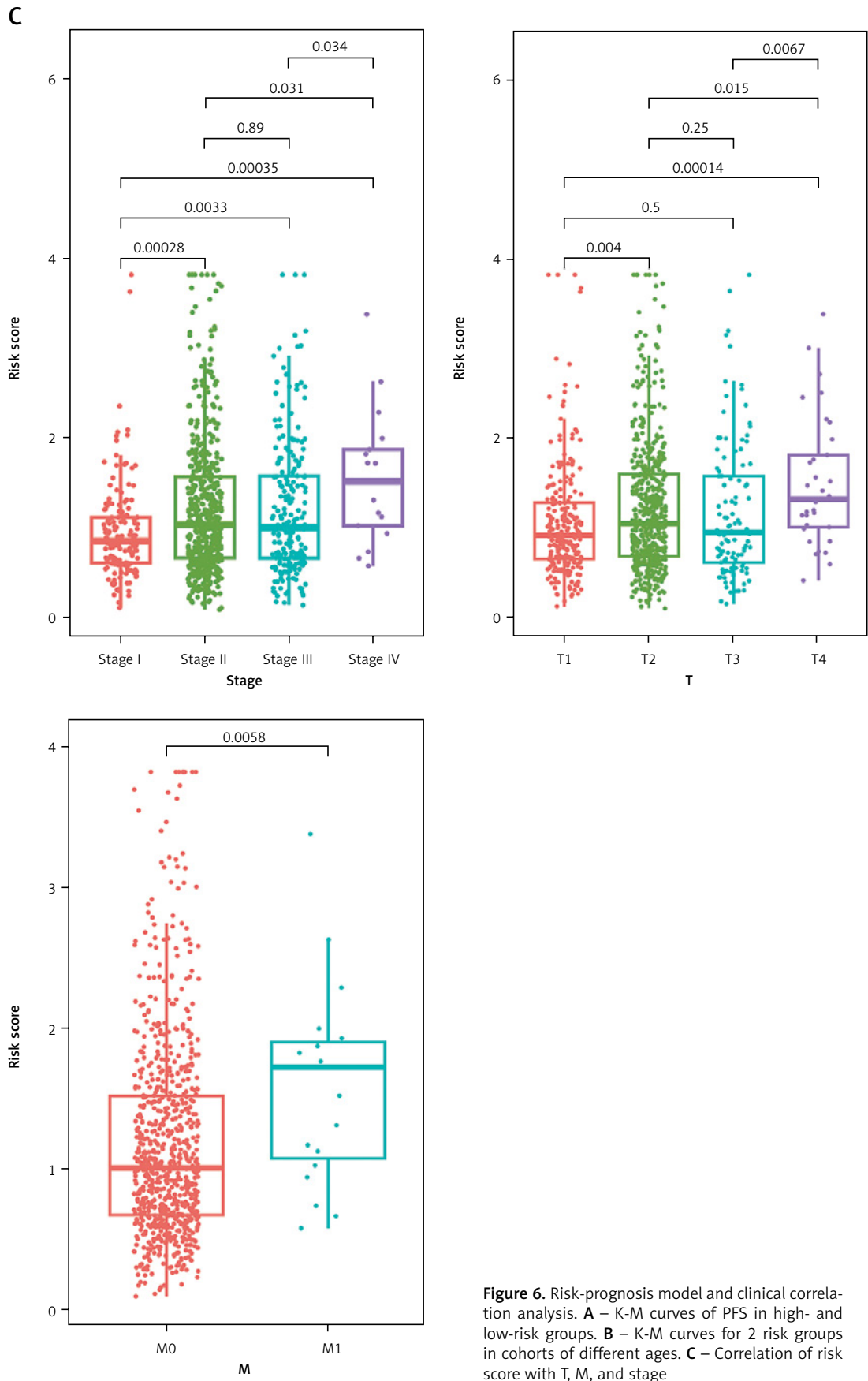


Figure 6. Risk-prognosis model and clinical correlation analysis. **A** – K-M curves of PFS in high- and low-risk groups. **B** – K-M curves for 2 risk groups in cohorts of different ages. **C** – Correlation of risk score with T, M, and stage

was significant enrichment of linoleic acid metabolism, complement and coagulation cascades, arachidonic acid metabolism, and PPAR signaling pathways for low-risk patients (Figure 7).

Characterization of the immune microenvironment for risk score

Given the pivotal role of the tumor immune microenvironment and the transformative impact of immune checkpoint drugs in cancer treatment, we investigated the relationship between the immune microenvironment and the risk score in all patients. Our analysis revealed that patients in the high-risk group exhibited significantly reduced percentages of naive B cells, CD8⁺ T cells, and resting dendritic cells, as depicted in Figures 8 A–C. Conversely, the proportions of M0 and M2 macrophages were notably higher in these patients, indicating that, in the high-risk group of patients, M0 is polarized to M2 in a greater proportion. Moreover, our examination of immune-related processes, such as the type I interferon (IFN) response, co-stimulation and co-inhibition of antigen-presenting cells (APCs), T cell co-inhibition, and regulatory T cells (Treg), revealed substantially higher activity in the high-risk group (Figure 8 D). Furthermore, our differential analysis of immune checkpoint genes indicated that the high-risk group exhibited higher expression levels of immune checkpoint-related genes. These included CD28, CD80, CD86, PDCD1LG2 (PD-L2), and NRP1 (Figure 8 E). Taken together, our findings suggest that patients in the high-risk group exhibit a suppressed immune response, characterized by reduced CD8⁺ T cell levels, likely driven by elevated

PD-L2 expression, which inhibits immune cell function. Additionally, high infiltration of regulatory T cells (Tregs) and M2 macrophages further suppresses effector T cell activity through the secretion of immunosuppressive cytokines such as IL-10 and TGF- β .

The mutational landscape, TMB, and drug susceptibility in high- and low-risk groups

We conducted an analysis of the TMB for each BRCA patient and compared the mutation frequencies of the top 15 mutated genes between the high-risk and low-risk groups. Among these highly mutated genes were PIK3CA, TP53, TTN, CDH1, GATA3, MUC16, KMT2C, MAP3K1, HMCN1, FLG, RYR2, SYNE1, USH2A, ZFH4, and PTEN. Notably, TP53, TTN, MUC16, and HMCN1 mutations were more prevalent in the high-risk group (Figures 9 A, B). Furthermore, we observed a significant difference in TMB between the two risk groups ($p < 0.001$, Figure 9 C). Interestingly, patients with lower TMB exhibited a more favorable prognosis (Figure 9 D). Importantly, those with both high TMB and high risk scores had the lowest chances of survival ($p < 0.001$, Figure 9 E). Additionally, when screening for sensitive drugs associated with risk scores, we discovered that patients in the low-risk group exhibited greater sensitivity to several targeted drugs. These included JAK1_870, KRAS (G12C) inhibitor-12, buparlisib, Wee1 inhibitor, afuresertib, and CDK9_5576. Moreover, patients in the low-risk group were also more responsive to certain common antitumor drugs such as leflunomide and oxaliplatin. To support the robustness of these findings, the confidence intervals for IC₅₀

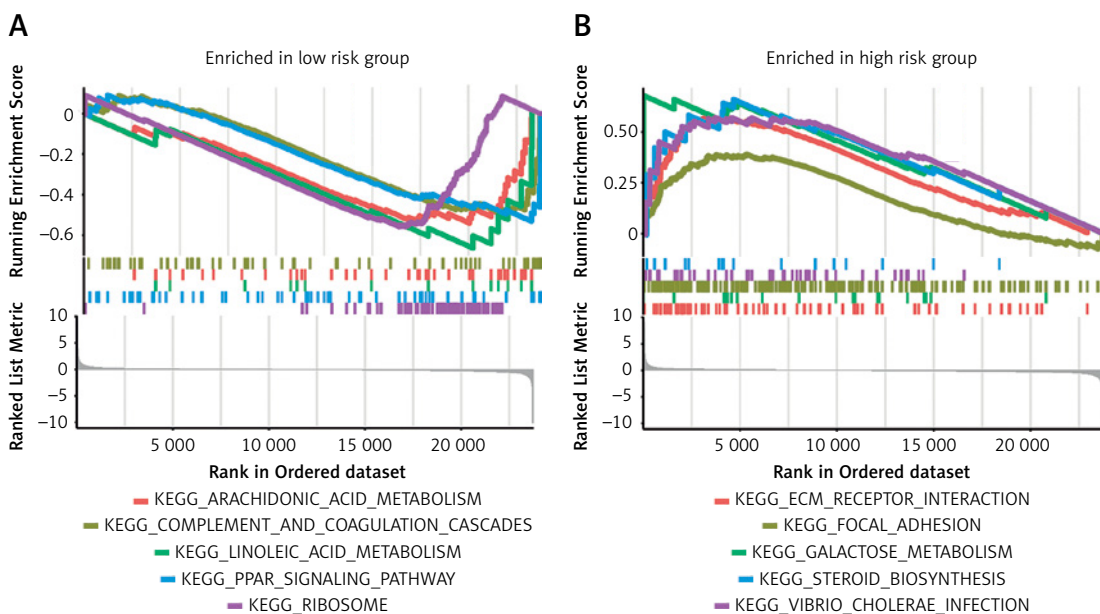


Figure 7. Gene set enrichment analysis in high- and low-risk groups. **A** – Top 5 pathways enriched in the high-risk group. **B** – Top 5 pathways enriched in the low-risk group

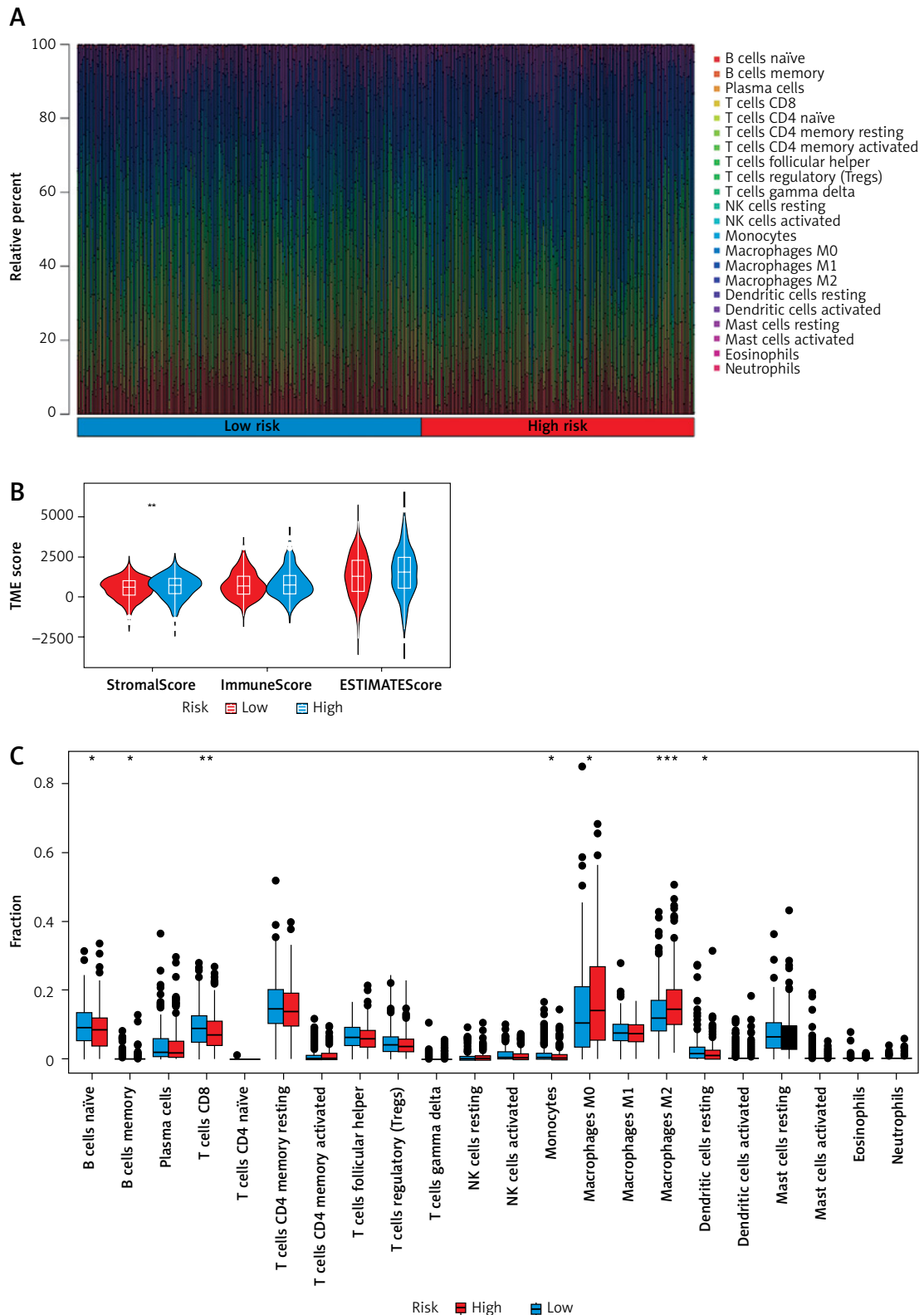


Figure 8. Immune landscapes for risk prognosis model. **A** – Relevant percentage of immune cell infiltration in high- and low-risk groups. **B** – Comparison of TME scores between the 2 risk groups. **C** – Differences in immune cell infiltration between the 2 risk groups. * $p < 0.05$; ** $p < 0.01$, *** $p < 0.001$

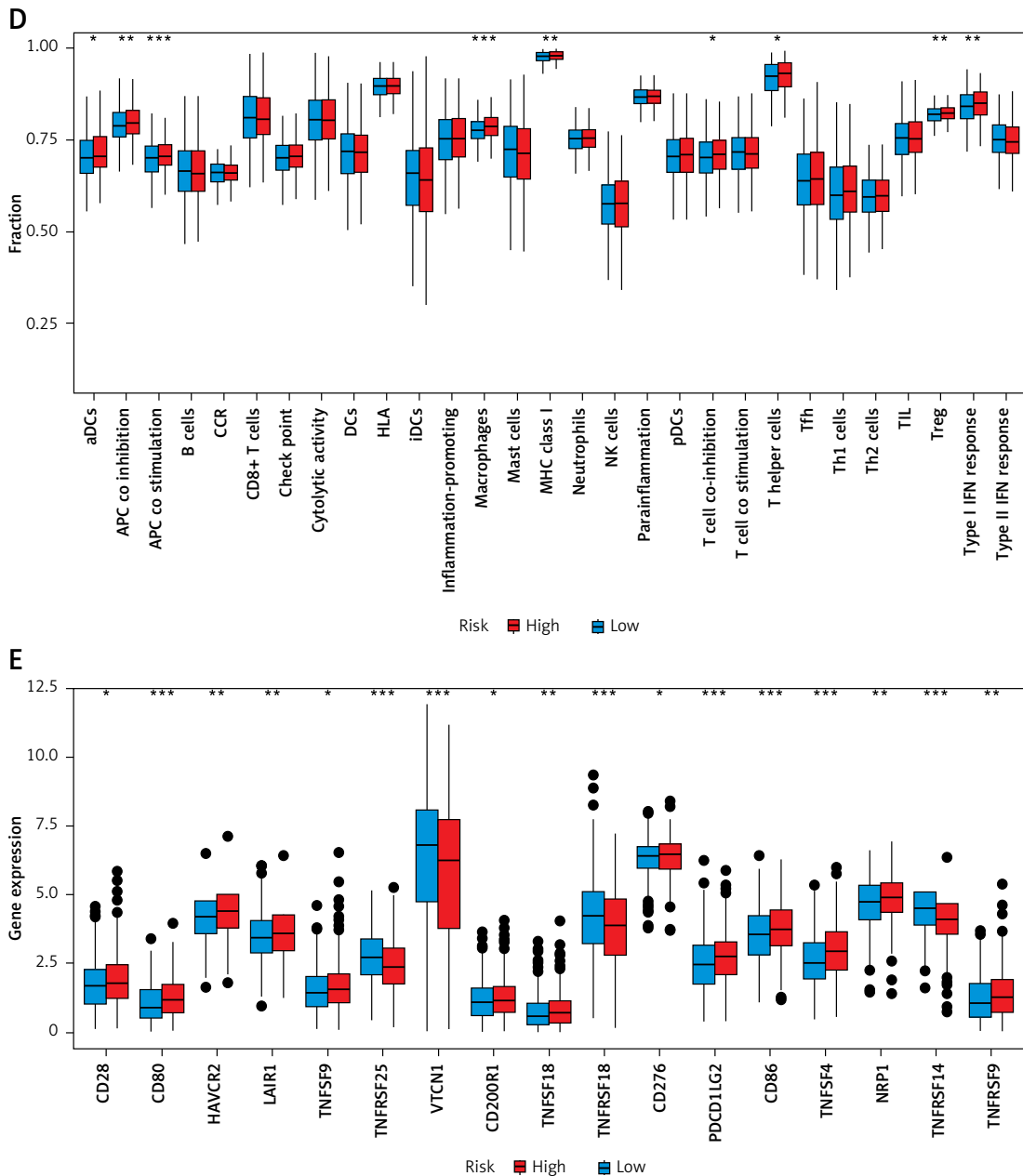


Figure 8. Cont. **D** – Differences in immune function between the 2 risk groups. **E** – Differences in common immune checkpoint genes between the 2 risk groups. * $p < 0.05$; ** $p < 0.01$, *** $p < 0.001$

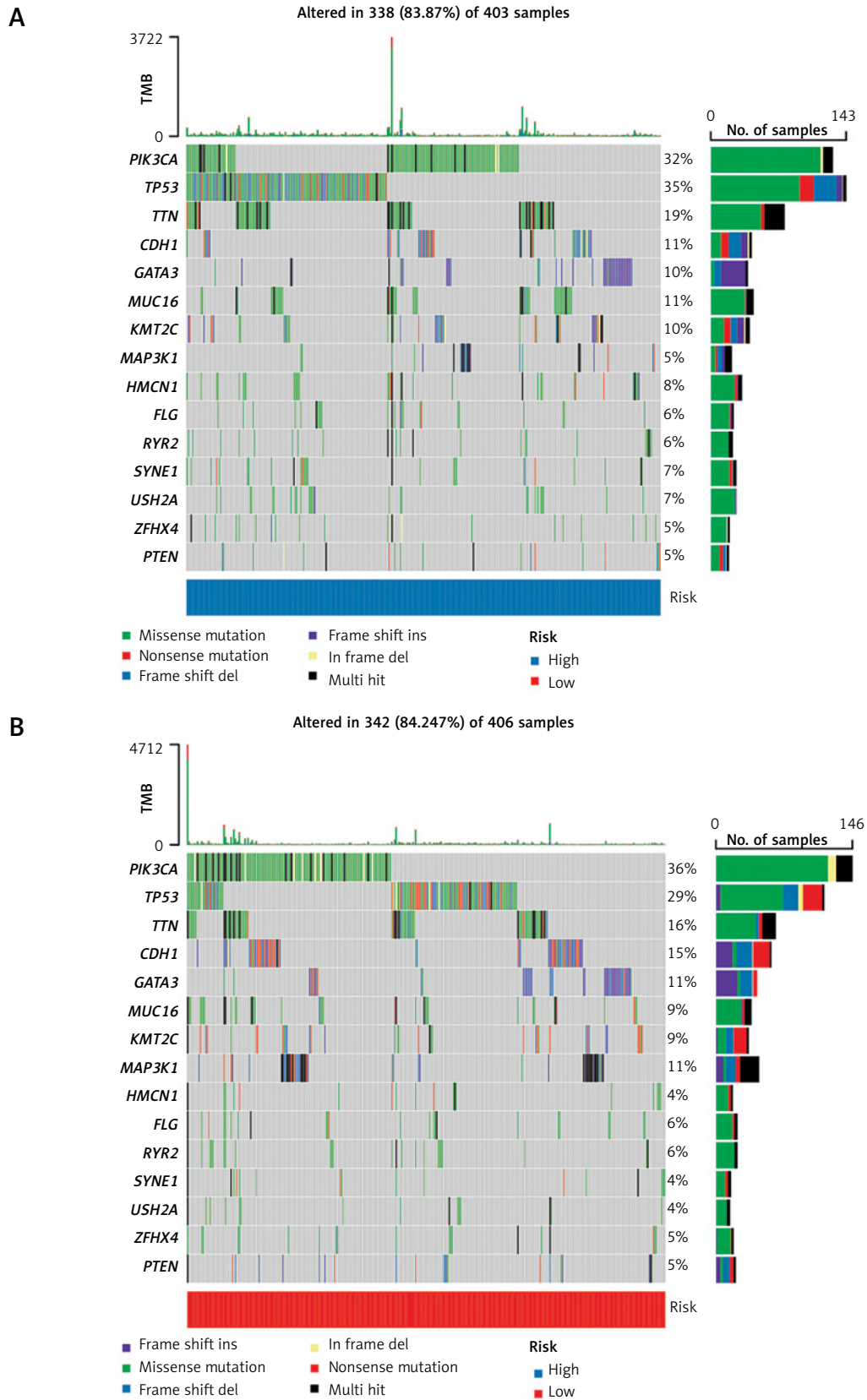
values of the drugs are provided in Supplementary Table SII. This suggests that the risk score can serve as a valuable guide for patients in selecting their drug regimen (Figure 9 F).

Discussion

As one of the most prevalent malignancies worldwide, BRCA poses a particularly significant challenge in China, where rising cases and fatalities demand urgent attention. Recognizing the potential therapeutic implications of disulfidptosis and the critical role of lncRNAs in BRCA, we have developed a prognostic model based on lncRNAs

associated with disulfidptosis to facilitate prognosis prediction.

In this study, based on the ten DRGs in the BRCA patients, consensus clustering was performed in this study to identify two distinct molecular clusters. The result showed that lower expression of DRGs was associated with better survival probability. GO and KEGG analyses revealed significant differences between the two clusters in terms of biological functions and signaling pathways. Notably, several immune-related pathways, the including humoral immune response, regulation of B cell activation, the B cell receptor signaling pathway, and the immunoglobulin complex, were



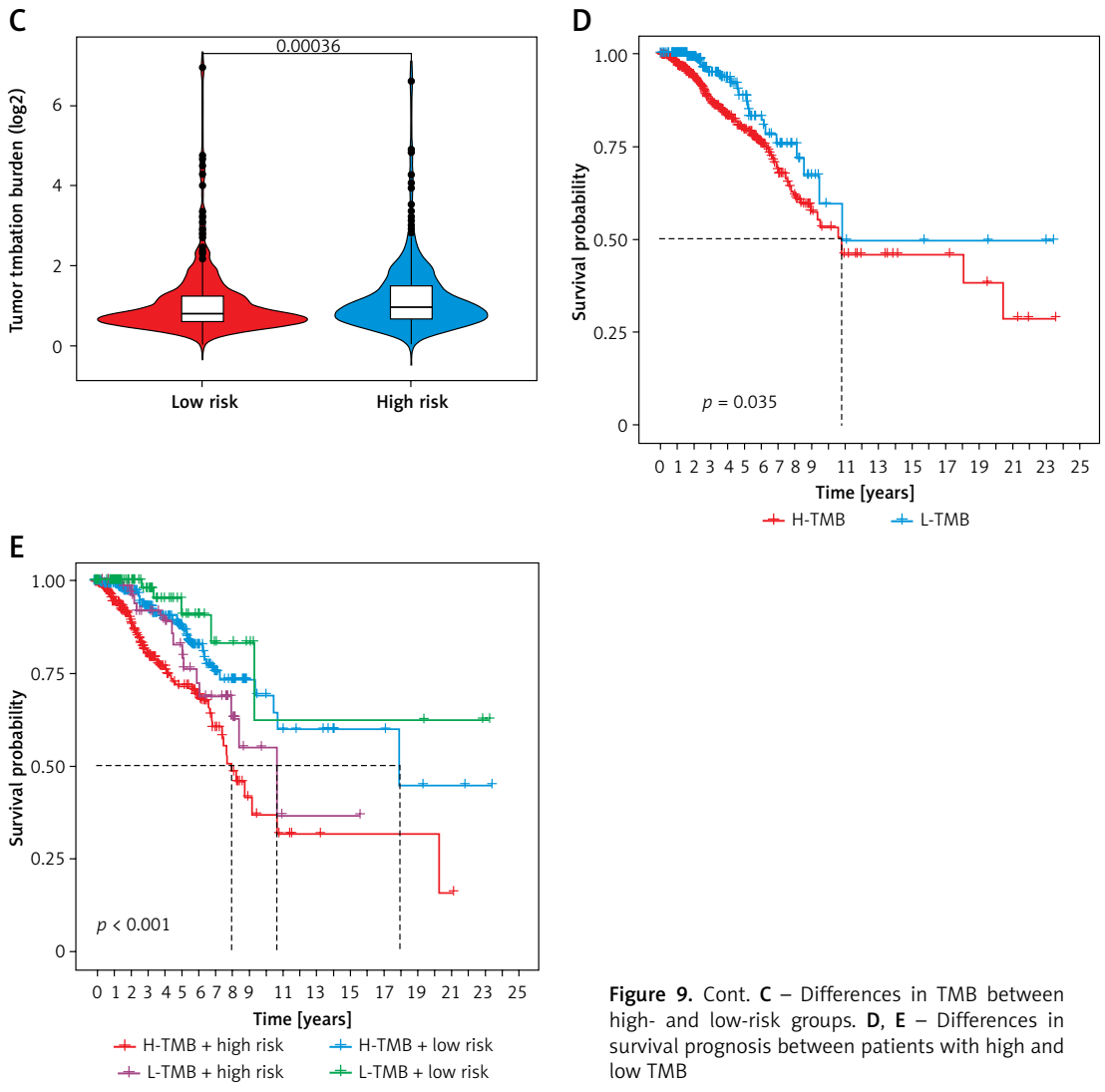


Figure 9. Cont. C – Differences in TMB between high- and low-risk groups. D, E – Differences in survival prognosis between patients with high and low TMB

significantly enriched. These findings underscore the potential link between DRGs and the immune microenvironment, warranting further in-depth investigation.

Building on the observed connections between DRGs and the immune microenvironment, we identified four DRlncRNAs (AC007996.1, AC004816.2, MIR200CHG, AL354920.1) to construct a robust prognostic model. The model was also validated as a potential independent prognostic factor for BRCA. MIR200CHG has been reported to influence the spread, invasion, and treatment response of BRCA [21]. Interestingly, two DRlncRNAs in the model, namely MIR200CHG and AC004816.2, have been included in other BRCA prediction models [20] and are all protective biomarkers, which is consistent with the findings of our study. While most identified DRlncRNAs align with existing models, AL354920.1 emerges as a novel marker, highlighting a promising avenue for future research. Given the novel association of MIR200CHG and AL354920.1 with BRCA

prognosis, further functional studies are essential to fully elucidate their roles in tumor progression and resistance to treatment. Such investigations may provide valuable insights into potential therapeutic targets for improving treatment outcomes in breast cancer.

We explored the correlation of risk score and clinicopathological characteristics. It was found that BRCA patients in the group with a high risk score were at an advanced tumor stage, which might have contributed to their poor prognoses. A nomogram serves as a predictive tool for assessing the prognosis of patients and can aid clinicians in making treatment decisions. To facilitate clinical decision-making, we constructed a nomogram. Additionally, to complement the nomogram and further evaluate the clinical utility of the predictive model, we employed the DCA curve. Our results demonstrate that the nomogram, which incorporates the risk score and clinical clinicopathological features, has significant potential for clinical decision-making, outperforming the

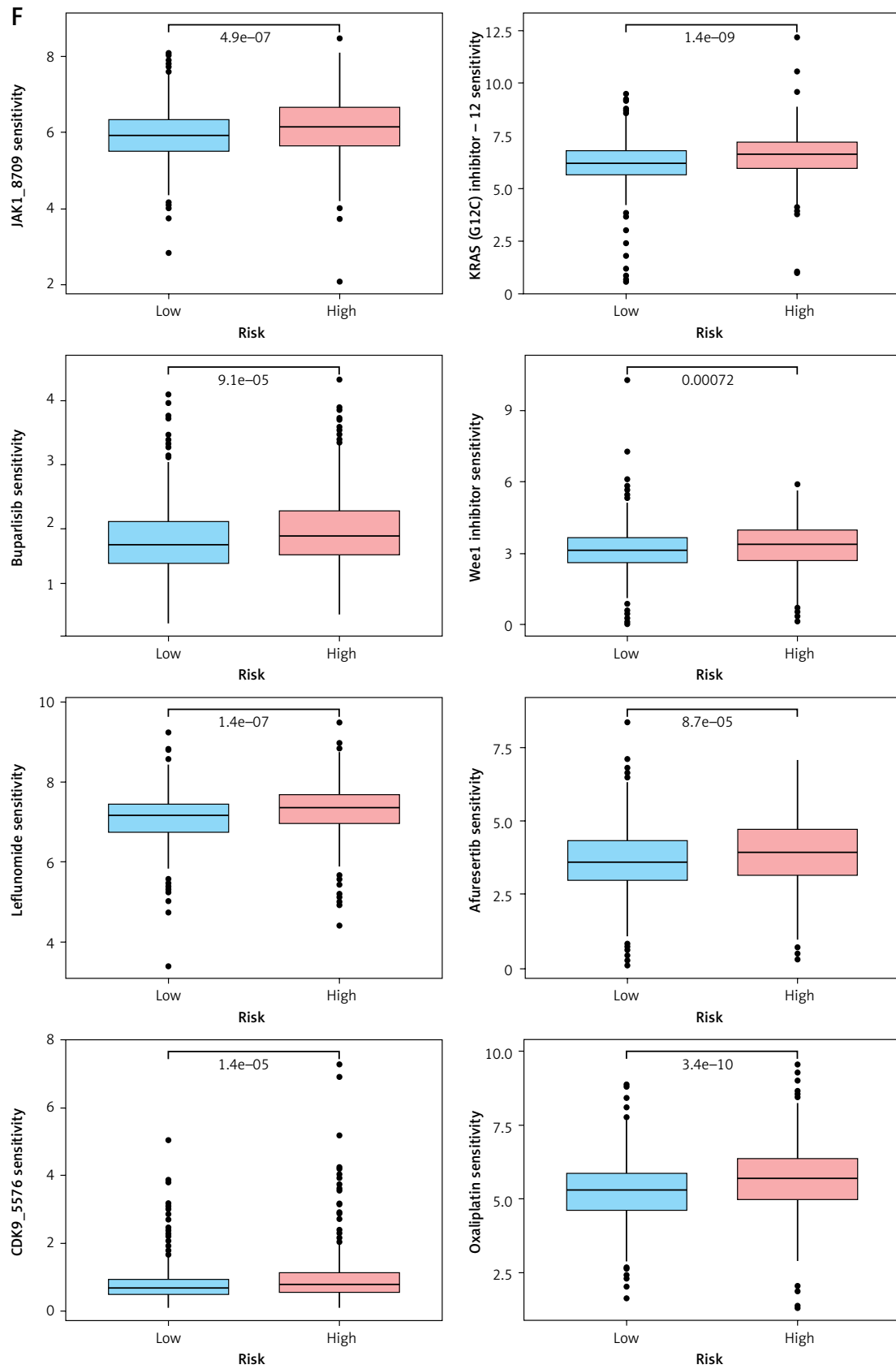


Figure 9. Cont. F – Drugs with differential sensitivity in high- and low-risk groups

risk score and stage individually. Therefore, we propose that the lncRNAs identified in this study have considerable potential for clinical translation, aiding treatment decisions. However, we must acknowledge challenges to their clinical application, including the high cost of detection technologies and the complexity of lncRNA detection and quantitative analysis. lncRNAs are often characterized by greater secondary structure variability and tissue specificity, which complicates detection. Further clinical validation is needed to confirm the reliability and stability of lncRNAs as biomarkers. In addition, although we conducted comprehensive internal validation to ensure the robustness of our model, we recognize that validation using independent GEO datasets would further enhance its generalizability. Unfortunately, no suitable external datasets with both disulfidptosis-related lncRNA expression and clinical information were available for this study.

The GSEA analysis showed that steroid biosynthesis, galactose metabolism, and ECM receptor interaction were enriched in the high-risk group. In contrast, linoleic acid metabolism, arachidonic acid metabolism, and the PPAR signaling pathway were activated in the low-risk group. There is evidence suggesting that steroid biosynthesis, galactose metabolism, and ECM receptor interaction are crucial for tumor growth and migration [22–24]. Interestingly, arachidonic acid metabolism and the PPAR signaling pathway are associated with various malignancies and inflammatory diseases [25–27]. Therefore, these pathways may offer potential therapeutic and preventive strategies for BRCA patients.

Individual differences in tumor progression exist due to heterogeneity in the tumor microenvironment [28, 29]. Therefore, it is necessary to develop activation strategies that target the immune microenvironment based on the different immune escape mechanisms in the TME. The results of our immune cell infiltration and functional analyses suggested that tumors in the high-risk group exhibited a poor immune response, accompanied by upregulation of major immune checkpoints, including the emerging gene PDCD1LG2. Specifically, compared to the low-risk scoring group, CD8⁺ T-cell infiltration was reduced in the high-risk scoring group, whereas the level of M2 infiltration was higher, and T-cell-coinhibition and Treg scores were higher in the high-risk scoring group. There are a number of mechanisms that inhibit T cell activity (e.g., reducing CD8⁺ T cell infiltration) in the tumor microenvironment, including activation of immune checkpoint pathways, such as PD-1, PD-L1, and PD-L2, which results in suppression of T cell function [30, 31], and activated Treg inhibit effector T cell activity by secreting inhibi-

tory cytokines, and direct cellular contact, which contributes to the tumor's escape from immune system surveillance [32]. In addition, polarized M2 macrophages are also involved in inhibiting the activation and proliferation of suppressor T cells. Tumor-associated macrophages (TAMs) are among the most abundant infiltrating leukocytes in various tumors. TAMs can be classified into two subtypes: M1-type and M2-type. M1-type TAMs exhibit anticancer activity by releasing nitric oxide (NO) and promoting a Th1/cytotoxic T cell response. In contrast, M2-type TAMs contribute to immunosuppression by either directly or indirectly inhibiting T cell function. This is achieved through the expression of immune checkpoint ligands such as PD-L1, secretion of inhibitory cytokines such as IL-10 and TGF- β , and suppression of T cell activity. This polarization of M2 is closely related to tumor progression and therapeutic resistance. Consequently, reprogramming M2-type TAMs to an M1-like phenotype has emerged as a promising therapeutic strategy to enhance T cell-mediated antitumor immunity and mitigate the immunosuppressive tumor microenvironment [33–36]. Our findings of higher level of M2 in the high-risk group indicate that this group of patients can benefit from M1 polarization therapy. However, further research is required to determine whether these findings can translate into promising antitumor therapies for BRCA.

As anticipated, the genes PIK3CA and TP53 exhibited the highest mutation rates in the two groups. PIK3CA mutations have a strong correlation with prognosis and treatment options for BRCA [37]. On the other hand, TP53, as a tumor suppressor gene, plays crucial roles in controlling the cell cycle, aging, and DNA repair [38, 39], and its significant impact has been extensively explored in various studies. Apart from PIK3CA and TP53, the discovery of elevated MAP3K1 mutations in the low-risk group underscores potential therapeutic distinctions between the clusters. MAP3K1 may indeed have an impact on the aggressiveness and treatment response in BRCA [40, 41]. Moreover, genomic studies have indicated that MAP3K1 mutations are particularly prevalent in the luminal A subtype of BRCA [42], which could be linked to the better prognosis observed in the low-risk group.

Clinically, treatment strategies for breast cancer have shown a diverse range of characteristics, encompassing endocrine therapy, targeted therapy, chemotherapy, and emerging immunotherapy approaches. The choice of therapeutic options depends on the molecular subtype of the tumor, the clinical stage of the patient, and the response to specific treatments. With the increasing understanding of the biological mechanisms underlying

breast cancer, numerous promising target genes have been identified and are currently being explored in clinical trials to assess the efficacy of their inhibitors. In our drug sensitivity analysis, we found that patients in the low-risk group exhibited greater sensitivity to several targeted therapies, including JAK1_870, KRAS (G12C) inhibitor-12, buparlisib, Wee1 inhibitor, afuresertib, and CDK9_5576. Additionally, patients in this group showed increased responsiveness to common antitumor agents such as oxaliplatin. Buparlisib, a PI3K inhibitor, has demonstrated clinical benefits in breast cancer in several clinical trials, particularly in patients with high rates of PIK3CA mutations, which sensitize breast cancer patients to buparlisib through PI3K activation [43–45]. In our study, the higher mutation rate of PIK3CA in the low-risk group may explain their enhanced sensitivity to buparlisib. This suggests that our risk model could potentially identify patients who are more likely to respond to buparlisib, aiding in personalized treatment plans and patient selection for clinical trials investigating buparlisib in breast cancer. Additionally, a recent study by Karen Cichowski *et al.* from Harvard Medical School, published in *Nature*, demonstrated that AKT and EZH2 inhibitors effectively target triple-negative breast cancers (TNBCs) by hijacking mechanisms of involution [46]. Moreover, several clinical trials are currently evaluating the safety and efficacy of afuresertib in breast cancer patients. The implementation of our risk model could support the design of clinical trials for afuresertib in this context. Similarly, drugs targeting JAK1_870, KRAS (G12C), CDK9_5576, and Wee1 are also in clinical trials, and incorporating our risk model could inform the design of these studies [47–49].

When comparing the 10-year C-index and AUC values for 1, 3, and 5 years, our model demonstrated stronger predictive power for 10-year overall survival (OS) in breast cancer patients than other disulfidptosis-related models. However, it showed slightly weaker performance in predicting OS during the first 5 years. Furthermore, in contrast to the models by Wang *et al.* [16], Zheng *et al.* [17], and Chen *et al.* [19], our study developed a novel disulfidptosis-related lncRNA model based on 10 disulfidptosis-related genes. Additionally, we constructed a nomogram integrating the risk score and clinical factors, which has significant potential for clinical decision-making. The results of the drug sensitivity analysis suggest that risk scores could be used to identify patients likely to respond to targeted therapies, as well as to guide clinical trials of these agents.

Our current study successfully constructed a prognostic model using four DRlncRNAs, demonstrating favorable predictive accuracy and stability.

Despite these promising findings, several limitations must be addressed to strengthen the model's clinical utility. First, the retrospective design of our study and the lack of external validation cohorts limit the generalizability of our model. In future research, prospective cohort evaluations are essential to validate its predictive power. Secondly, the gene expression results in tumor and normal tissues showed inconsistencies between TCGA and qRT-PCR. This discrepancy could be attributed to biological variability among populations from different regions, the limited sample size in qRT-PCR validation, and technical differences between high-throughput sequencing and qRT-PCR platforms. Future studies should validate these findings in larger cohorts from diverse regions. Thirdly, while immune checkpoint inhibitor (ICI)-based immunotherapy and readily available medications have shown therapeutic potential for different groups, further research is needed to determine the optimal treatment regimen selection. Finally, potential overfitting in LASSO regression may arise due to the limited number of DRlncRNAs. We plan to address this concern in future work by incorporating additional validation to assess the robustness of our thresholds.

In conclusion, we developed a novel prognostic model based on four disulfidptosis-related lncRNAs (DRlncRNAs: AC007996.1, AC004816.2, MIR200CHG, and AL354920.1) for predicting breast cancer (BRCA) prognosis. This model effectively stratifies patients into high-risk and low-risk groups, with high-risk patients showing significantly poorer overall survival, increased tumor mutational burden (TMB), and a more immunosuppressive tumor microenvironment. Furthermore, high-risk patients exhibited elevated expression of immune checkpoint genes, while low-risk patients demonstrated greater sensitivity to specific targeted therapies, suggesting that the risk score could serve as a potential tool for predicting response to immune checkpoint blockade (ICB) therapy and several antitumor drugs. Our findings suggest that our model could serve as a valuable tool for prognosis prediction and guiding personalized treatment strategies in BRCA.

Acknowledgments

Qinghua Zhang, Guizhen Pan and Tingting Wang contributed equally to this work.

Data availability and materials

The original contributions presented in the study are included in the article/Supplementary Material. Further inquiries can be directed to the corresponding author. The public data cohorts analyzed in this study are available from TCGA

(<https://portal.gdc.cancer.gov/>). R and other customs scripts for analyzing data are available from the corresponding author on reasonable request.

Funding

The authors disclosed receipt of the following financial support for the research, authorship, and/or publication of this article: This study was supported by the National Natural Science Funds of China (No. 82172775), National Key Clinical Specialty Construction Project 2021 Oncology (No. 2021GJLC01) and Anhui Province Cancer Bioimmunotherapy Clinical Medical Research Center (No. 202101B10202005). The funders only provided financial support.

Ethical approval

Breast cancer tissues and normal tissues were collected from Anhui Provincial Hospital. In addition, for investigations involving human subjects, informed consent has been obtained from the participants involved. The project was approved by the ethics committee of Anhui Provincial Hospital (2023-ZNW-04).

Conflict of interest

The authors declare no conflict of interest.

References

1. Miller KD, Nogueira L, Devasia T, et al. Cancer treatment and survivorship statistics, 2022. *CA Cancer J Clin* 2022; 72: 409-36.
2. Siegel RL, Miller KD, Fuchs HE, Jemal A. Cancer statistics, 2022. *CA Cancer J Clin* 2022; 72: 7-33.
3. Badowska-Kozakiewicz AM, Budzik MP, Liszcz A, et al. Clinicopathological factors associated with novel prognostic markers for patients with triple negative breast cancer. *Arch Med Sci* 2019; 15: 1433-42.
4. Liu YB, Gao XT, Huang LY, Liu XL. Clinicopathological characteristics and prognostic factors in invasive micropapillary carcinoma of the breast. *Arch Med Sci* 2024; 20: 428-35.
5. Yang G, Lu X, Yuan L. LncRNA: a link between RNA and cancer. *Biochim Biophys Acta* 2014; 1839: 1097-109.
6. Yin Z, Wang J, Zhu C, Xu C, Fang J, Li Q. Identification and verification of a novel disulfidptosis-related lncRNAs prognostic signature to predict the prognosis and immune activity of head and neck squamous carcinoma. *Iran J Public Health* 2024; 53: 2328-40.
7. Lin J, Lin N, Zhao W. Development and validation of a prognostic nomogram for lower-grade glioma based on an autophagy-related lncRNA signature. *Arch Med Sci* DOI: <https://doi.org/10.5114/aoms/145435>.
8. Lu R, Zhang J, Zhang W, et al. Circulating HOTAIR expression predicts the clinical response to neoadjuvant chemotherapy in patients with breast cancer. *Cancer Biomark* 2018; 22: 249-56.
9. Özgür E, Ferhatoğlu F, Şen F, Saip P, Gezer U. Circulating lncRNA H19 may be a useful marker of response to neoadjuvant chemotherapy in breast cancer. *Cancer Biomark* 2020; 27: 11-7.
10. Elhasnaoui J, Miano V, Ferrero G, et al. DSCAM-AS1-driven proliferation of breast cancer cells involves regulation of alternative exon splicing and 3'-end usage. *Cancers (Basel)* 2020; 12: 1453.
11. Jiang W, Pan S, Chen X, Wang ZW, Zhu X. The role of lncRNAs and circRNAs in the PD-1/PD-L1 pathway in cancer immunotherapy. *Mol Cancer* 2021; 20: 116.
12. Tsvetkov P, Coy S, Petrova B, et al. Copper induces cell death by targeting lipoylated TCA cycle proteins. *Science* 2022; 375: 1254-61.
13. Liu X, Nie L, Zhang Y, et al. Actin cytoskeleton vulnerability to disulfide stress mediates disulfidptosis. *Nat Cell Biol* 2023; 25: 404-14.
14. He WP, Chen YY, Wu LX, Guo YY, You ZS, Yang GF. A novel necroptosis-related lncRNA signature for predicting prognosis and anti-cancer treatment response in endometrial cancer. *Front Immunol* 2022; 13: 1018544.
15. Cui H, Lian J, Xu B, et al. Identification of a bile acid and bile salt metabolism-related lncRNA signature for predicting prognosis and treatment response in hepatocellular carcinoma. *Sci Rep* 2023; 13: 19512.
16. Wang J, Zheng Q, Jian J, et al. Construction of a disulfidptosis-associated lncRNA signature to predict prognosis in bladder cancer. *Transl Androl Urol* 2024; 13: 2705-23.
17. Zheng Y, Lin Y, Zhang Y, Liu S, Yang Y, Huang W. Determining new disulfidptosis-associated lncRNA signatures pertinent to breast cancer prognosis and immunological microenvironment. *Transl Cancer Res* 2024; 13: 5815-29.
18. Liu S, Zheng Y, Li S, et al. Integrative landscape analysis of prognostic model biomarkers and immunogenomics of disulfidptosis-related genes in breast cancer based on LASSO and WGCNA analyses. *J Cancer Res Clin Oncol* 2023; 149: 16851-67.
19. Chen X, Yang C. A novel disulfidptosis-related lncRNAs prognostic signature for prognosis predicting and immune microenvironment characterization in breast cancer. *Curr Med Chem* 2024. doi: 10.2174/0109298673294711240405090150.
20. Wu J, Cai Y, Zhao G. Identification of disulfidptosis-related clusters and construction of a disulfidptosis-related gene prognostic signature in triple-negative breast cancer. *Heliyon* 2024; 10: e33092.
21. Tang L, Wei D, Xu X, et al. Long non-coding RNA MIR200CHG promotes breast cancer proliferation, invasion, and drug resistance by interacting with and stabilizing YB-1. *NPJ Breast Cancer* 2021; 7: 94.
22. Capper CP, Rae JM, Auchus RJ. The metabolism, analysis, and targeting of steroid hormones in breast and prostate cancer. *Horm Cancer* 2016; 7: 149-64.
23. Cramer DW, Harlow BL, Willett WC, et al. Galactose consumption and metabolism in relation to the risk of ovarian cancer. *Lancet* 1989; 2: 66-71.
24. Bao Y, Wang L, Shi L, et al. Transcriptome profiling revealed multiple genes and ECM-receptor interaction pathways that may be associated with breast cancer. *Cell Mol Biol Lett* 2019; 24: 38.
25. Yarla NS, Bishayee A, Sethi G, et al. Targeting arachidonic acid pathway by natural products for cancer prevention and therapy. *Semin Cancer Biol* 2016; 40-41: 48-81.
26. Fanale D, Amodeo V, Caruso S. The interplay between metabolism, PPAR signaling pathway, and cancer. *PPAR Res* 2017; 2017: 1830626.

27. Wang B, Wu L, Chen J, et al. Metabolism pathways of arachidonic acids: mechanisms and potential therapeutic targets. *Signal Transduct Target Ther* 2021; 6: 94.
28. Junttila MR, de Sauvage FJ. Influence of tumour micro-environment heterogeneity on therapeutic response. *Nature* 2013; 501: 346-54.
29. Pan G, Xie H, Xia Y. Disulfidptosis characterizes the tumor microenvironment and predicts immunotherapy sensitivity and prognosis in bladder cancer. *Heliyon* 2024; 10: e25573.
30. Liu C, Somasundaram A, Manne S, et al. Neuropilin-1 is a T cell memory checkpoint limiting long-term antitumor immunity. *Nat Immunol* 2020; 21: 1010-21.
31. Chuckran CA, Liu C, Bruno TC, Workman CJ, Vignali DA. Neuropilin-1: a checkpoint target with unique implications for cancer immunology and immunotherapy. *J Immunother Cancer* 2020; 8: e000967.
32. Ohue Y, Nishikawa H. Regulatory T (Treg) cells in cancer: can Treg cells be a new therapeutic target? *Cancer Sci* 2019; 110: 2080-9.
33. Fu LQ, Du WL, Cai MH, Yao JY, Zhao YY, Mou XZ. The roles of tumor-associated macrophages in tumor angiogenesis and metastasis. *Cell Immunol* 2020; 353: 104119.
34. Wang Y, Smith W, Hao D, He B, Kong L. M1 and M2 macrophage polarization and potentially therapeutic naturally occurring compounds. *Int Immunopharmacol* 2019; 70: 459-66.
35. Nowak M, Klink M. The role of tumor-associated macrophages in the progression and chemoresistance of ovarian cancer. *Cells* 2020; 9: 1299.
36. Wei Z, Zhang X, Yong T, et al. Boosting anti-PD-1 therapy with metformin-loaded macrophage-derived microparticles. *Nat Commun* 2021; 12: 440.
37. Mukohara T. PI3K mutations in breast cancer: prognostic and therapeutic implications. *Breast Cancer (Dove Med Press)* 2015; 7: 111-23.
38. Zhang Y, Xiong S, Liu B, et al. Somatic Trp53 mutations differentially drive breast cancer and evolution of metastases. *Nat Commun* 2018; 9: 3953.
39. Badve SS, Gökmen-Polar Y. TP53 status and estrogen receptor-beta in triple-negative breast cancer: company matters. *J Natl Cancer Inst* 2019; 111: 1118-9.
40. Pham TT, Angus SP, Johnson GL. MAP3K1: genomic alterations in cancer and function in promoting cell survival or apoptosis. *Genes Cancer* 2013; 4: 419-26.
41. Avivar-Valderas A, McEwen R, Taheri-Ghahfarokhi A, et al. Functional significance of co-occurring mutations in PIK3CA and MAP3K1 in breast cancer. *Oncotarget* 2018; 9: 21444-58.
42. Banerji S, Cibulskis K, Rangel-Escareno C, et al. Sequence analysis of mutations and translocations across breast cancer subtypes. *Nature* 2012; 486: 405-9.
43. Fuso P, Muratore M, D'Angelo T, et al. PI3K inhibitors in advanced breast cancer: the past, the present, new challenges and future perspectives. *Cancers (Basel)* 2022; 14: 2161.
44. Garrido-Castro AC, Saura C, Barroso-Sousa R, et al. Phase 2 study of buparlisib (BKM120), a pan-class I PI3K inhibitor, in patients with metastatic triple-negative breast cancer. *Breast Cancer Res* 2020; 22: 120.
45. Pistilli B, Pluard T, Urruticochea A, et al. Phase II study of buparlisib (BKM120) and trastuzumab in patients with HER2+ locally advanced or metastatic breast cancer resistant to trastuzumab-based therapy. *Breast Cancer Res Treat* 2018; 168: 357-64.
46. Schade AE, Perurena N, Yang Y, et al. AKT and EZH2 inhibitors kill TNBCs by hijacking mechanisms of involution. *Nature* 2024; 635: 755-63.
47. Stover DG, Gil Del Alcazar CR, Brock J, et al. Phase II study of ruxolitinib, a selective JAK1/2 inhibitor, in patients with metastatic triple-negative breast cancer. *NPJ Breast Cancer* 2018; 4: 10.
48. Teo ZL, O'Connor MJ, Versaci S, et al. Combined PARP and WEE1 inhibition triggers anti-tumor immune response in BRCA1/2 wildtype triple-negative breast cancer. *NPJ Breast Cancer* 2023; 9: 68.
49. Ji D, Luo Y, Wang J, et al. CDK4/6 inhibitors, PI3K/mTOR inhibitors, and HDAC inhibitors as second-line treatments for hormone receptor-positive, HER2-negative advanced breast cancer: a network meta-analysis. *BMC Cancer* 2023; 23: 805.